4-1-2022

Jet engine emissions and vapor contrail reduction through increased combustion efficiency with the aim to mitigate greenhouse gases emissions

Austin J. Brant
Georgia Southern University

Jet engine emissions and vapor contrail reduction through increased combustion efficiency with the aim to mitigate greenhouse gases emissions

An Honors Thesis submitted in partial fulfillment of the requirements for Honors in *Mechanical Engineering.*

By *Austin Brant*

Under the mentorship of *Dr. Valentin Soloiu*

As society continues to globalize and advance in complexity, the increased demand for business aviation has caused the global travel rate of airlines to increase with each year. With this continual increase in aviation travel, the Federal Aviation Administration (FAA) predicts that the fuel consumption rate is to increase by 1.6 percent as of the year 2025. While this increase in fuel consumption is a positive trait of a thriving aviation community, concerns also arise regarding increased greenhouse gas emissions and enlarged contributions to the greenhouse effect. The most prevalent greenhouse gases associated with jet engine emissions are water vapor, carbon dioxide, carbon monoxide, nitrogen oxides, and small soot particulates. A solution to this growing issue is the use of synthetic fuels as an alternative to traditional fossil fuels which emit significantly less greenhouse gases. The research performed in this paper found that the combustion of S8 produced greater magnitudes of vibrations than the combustion of Jet A but was also quieter and produced less emissions. Through the combustion process in the single-stage turbojet engine, S8 emitted 61.22% less water vapor, 5.31% less carbon dioxide gas, 18.18% less carbon monoxide emissions, 3.64% less nitrous oxide emissions, and lastly 133.33% less unburned hydrocarbons than Jet A.

Thesis Mentor:_____

Dr. *Valentin Soloiu*

Honors Director:_____

Dr. Steven Engel

April 2022

Department of Mechanical Engineering

University Honors Program

Georgia Southern University

Acknowledgements

I would like to give special thanks to my faculty mentor Dr. Valentin Soloiu for the countless hours and effort he has dedicated to training and teaching me. I am very thankful for the opportunity Dr. Soloiu has given me to perform research with him and thank God first and foremost along with Dr. Soloiu for giving me the skills to work with Gulfstream Aerospace Corporation. I would also like to thank all the lab members who have helped me complete experimental procedures and encourage me along the way in my research, especially Cesar Carapia, Levi McKinney, James O'Hara, David Obando, Trevor Carlton, Kody Pierce, John William McAfee, Richard Smith, Amanda Weaver, Lily Parker, Dillan Brock, Aidan Rowell, Drake Grall, Camille Phillips, Shaen Mehrzed, and Suraj Patel. Thank you all for the countless hours of friendship and comradery we have shared over the years performing research together.

I would also like to thank the Faculty and Department of Engineering for the support, time, and resources in which they have poured into my educational career at Georgia Southern. I would also like to thank the Georgia Southern University Honors Program for the assistance and encouragement which they have showed me during my time at Georgia Southern University.

Finally, I would like to thank my family, Kiera Ferrell, and best friend Matthew Kessler for all the support and encouragement you have poured onto me over the years and thank you for pushing me to be my best self-daily.

This research was supported by DoD-NSF Assure REU Site Award: 1950207 and experimental fuel contributions from the Air Force Research Laboratory

Table of Contents

List of Figures 1

List of Tables

1. Introduction

The objective of this study was to investigate the noise, vibrations, and emissions produced from the combustion of the synthetic kerosene Syntroleum 8 (S8) in comparison to the traditional fossil fuel-based kerosene, Jet A. S8 and Jet A were both combusted in a single-stage turbojet engine along with other fuel testing equipment to investigate each fuels' properties.

1.1 Fuels

According to the U.S. Energy Information Administration, the consumption of jet fuel on August 16th, 2020 was approximately 612,000 barrels which was only 43% of the entire quantity consumed a year earlier. As the world continues to return to the normal travel rates seen before the COVID-19 pandemic, the United States rate of return to normal fuel consumption is the fastest in the world only to China (Barnett, 2020). As the United States and World continue to consume jet fuels in extreme quantities, it is imperative that the qualities of the fuels being consumed are evaluated to protect the environment and reduce the overall greenhouse effect.

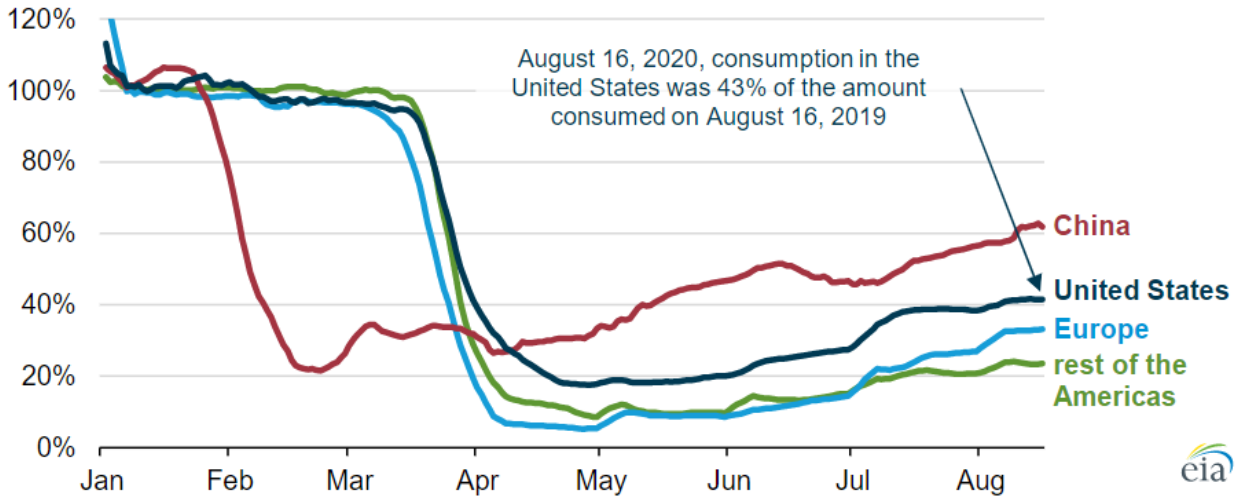

Figure 1. Jet Fuel Consumption Rate of United States and World (Barnett, 2020)

The conventional aviation fuels applied across North America, such as Jet A, are derived from the refining of crude oil and can be referred to as petroleum-derived jet fuels. As the concentrations of crude oils can be largely different due to the origin and extraction techniques of the oil, many different final jet fuel products can be produced (Satcher, 1993). Petroleum-derived jet fuels consist of large quantities of hydrocarbons and upon the combustion of these fuels, harmful emissions such as carbon dioxide (CO_2), nitrogen oxides (NO_x), sulfate and particulate matters, and water vapors are released into the atmosphere (Blakey, 2011). Jet A is the standard jet fuel across North America and serves as a benchmark fuel in which to compare alternative synthetic jet fuels (Hileman, 2009).

To improve the overall air quality and emissions produced by combustion, large quantities of sustainable aviation fuels (SAF's) are required to substitute or work in hand with conventional fuels in the future (Huq, 2021). SAF fuels are sustainable compared to traditional aviation fuels because of the large range of feedstocks in which they can be derived when compared to conventional fossil-based fuels. Syntroleum 8 which is better known as S8, is a synthetic paraffinic kerosene (SPK) which is derived from the liquification of natural gas and contains far less carbon and aromatics which are known to pollute the air. Fully synthetic fuels such as S8 pose as a solution to counteract the large dependence of the United States and World on conventional fossil fuels while also helping to improve combustion emissions and the overall air quality.

Fuel Property	Jet A (POSF 10325)	S8 (POSF 5018)
Flash Point, °C	38	48
Density (g/cm^3)	.775-.84	.756
Molecular Weight (g/mol)	159	166
Neat Heat of Combustion (MJ/Kg)	42.8	43.9
H Content (mass %)	14.0	15.2
Freeze Point, °C	-40	-49
DCN	48.8	60

Table 1. Fuel Properties of Jet A and S8 (Edwards, 2020)

As can be further evaluated in Table 1. above the fuel properties such as the flash point, density molecular weight, neat heat of combustion, hydrogen content, freeze point, and derived cetane number (DCN) of Jet A and S8 are listed (Edwards, 2020). From the evaluation of each fuel, it was found in a study by Edwards et al. that S8 had a higher flash point than Jet A and consequently freezes at nine degrees cooler than Jet A at -49 °C. In this study it was also found that the densities of both Jet A and S8 were near identical but S8 consisted of a higher molecular weight than Jet A. Regarding the neat heat of combustion and derived cetane number, S8 had higher neat heat of combustion values and cetane number in comparison to Jet A. Derived from the Hydrogen to Carbon ratio, S8 consisted of a higher percentage of Hydrogen compared to Jet A.

In this research, the synthetic fuel S8 which is derived during a gas to liquid (GTL) process known as Bio-Synfining™ was compared to the conventional aviation fuel Jet A. The known properties of each fuel such as the density, viscosity, paraffin content, and aromatic contents will

be evaluated to better understand the experimental vibrations, sound pressure, and emissions measured from the combustion of Jet A and S8.

1.2 Emissions

As the World and the United States continue to resume normal rates of travel post COVID-19, the levels of Greenhouse gas emissions are predicted to continually rise. According to the Federal Aviation Administration (FAA), the growth of the U.S. carrier domestic passenger services is to continue at a rate of approximately 2.3 percent throughout the year 2041 (Schaufele, 2021). While growth within the civil aviation sector is a sign of a thriving economy and society, a proportional growth in the amount of greenhouse gases emitted into the atmosphere will also be seen. The Greenhouse effect occurs when Greenhouse gasses in the atmosphere such as carbon dioxide (CO_2), nitrous oxides (NO_x), methane, and water vapor trap radiated heat from the sun within the Earth's atmosphere.

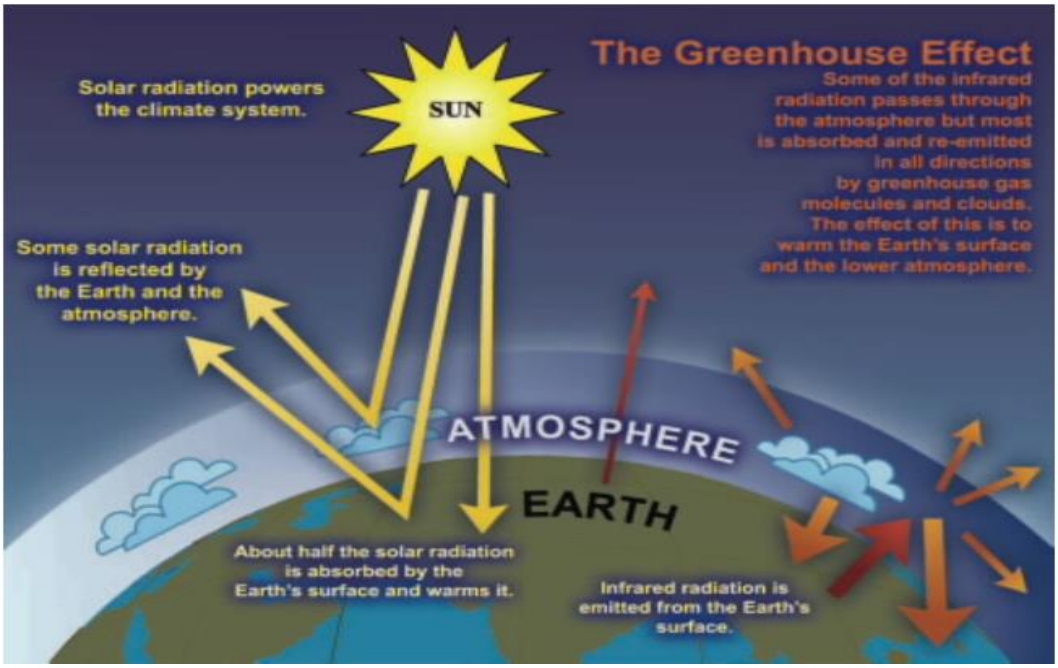

Figure 2. Global Greenhouse Effect Diagram (What is the Greenhouse Effect, 2022)

Greenhouse gasses such as carbon dioxide and water vapor are two of the most prevalent byproducts of combustion and can remain in the atmosphere from a couple of days to thousands of years before leaving the atmosphere. Because water is a decomposable gas, it only requires nine days before it will exit the atmosphere, whereas carbon dioxide can remain in the atmosphere for thousands of years because it is a non-decomposable gas (Buis, 2022). As the global carbon dioxide levels continue to escalate each year elevating the effects of the greenhouse effect, a proportional amount of water vapor is capable of evaporating into the hotter atmospheric temperature. According to NASA, while the emission of human contributed CO_2 and methane are contributing to increased global temperatures, water vapor is supercharging the global temperature rise (Buis, 2022).

Combustion in the most basic form is the process of burning a given fuel source, and a common characteristic amongst nearly all instances of combustion is the production of noise. When combustion is viewed regarding the turbo-jet engine, air is compressed by the compressor mechanism of the turbine and burnt as an air fuel mixture at the combustor to produce thrust. During the combustion process, a pressure changes from high pressures at combustion to low pressures at the exhaust naturally create large amounts of noise until equilibrium pressure is reached. Noise production can also be attributed to the unsteady combustion, or inconsistent burn of a fuel during the combustion process (Howe, 2010). While synthetic fuels produce less amounts of harmful emissions, such as carbon dioxide, nitrous gasses, and water vapor, the combustion of these fuels is not always as steady when compared to traditional fossil fuels such as Jet-A. Through the application of measurement microphones in this experimentation, the combustion irregularities of S8 will be measured and compared to those of Jet-A

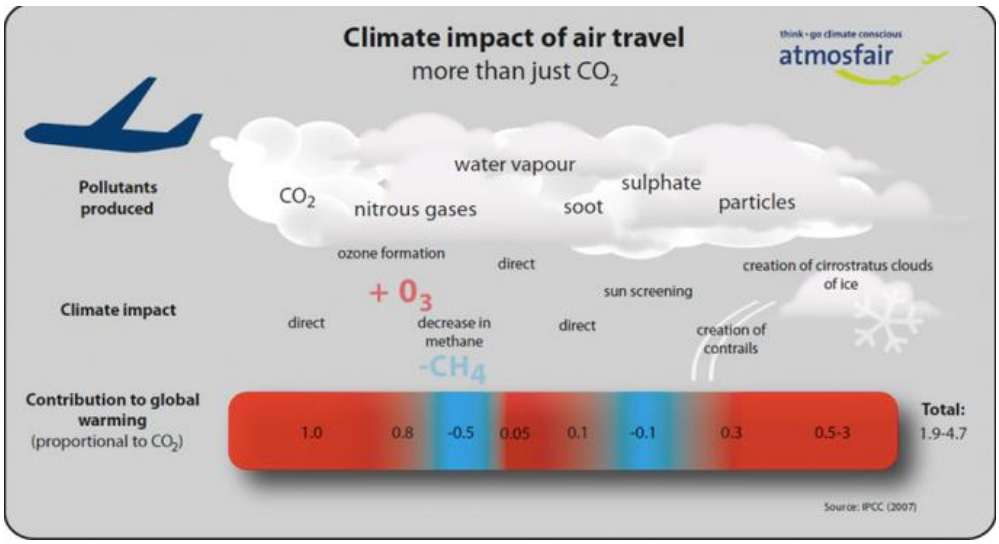

Figure 3. Aviation Emissions Species (Overton, 2019)

Vibrations attributed with the combustion process are of similar origin to the noise produced during combustion. When unsteady combustion or combustion irregularities are present, vibrations are produced from the incomplete or harsh combustion of the unburnt fuels (Octave Analysis, 2022). While synthetic fuels produce less harmful emissions when compared to traditional fossil fuels, the combustion of these fuels is not always as steady which leads to larger magnitudes of vibrations to be produced. Vibrations can also be produced through the presence of imbalanced components of a member which will lead to harmful wear of the member under evaluation.

The most prominent Greenhouse gases produced during the combustion of aviation fuels include carbon dioxide (CO_2), nitrous oxides (NO_x), soot and sulfate particulates, and water vapor (H_2O) which contributes to the formation of water vapor contrails (Lee, 2009).

1.3 Noise, Vibrations, and Harshness Analysis

Sounds can be defined as any pressure variation that the human ear is capable of detecting (Mahashabde, 2011). While some sounds are considered as pleasant or welcomed, others can cause discomfort or pain to the observer. Sounds that are generally considered to be unwanted or destructive are referred to as Noise and in most systems, the objective is to eliminate the presence of noise. There are two main forms of hearing loss in which noise can affect an individual, through a short exposure to a great impulse or extended exposure to a substantial level of noise. For example, a quick but intense gunshot without the proper ear protection can cause hearing damage to the observer as well as the prolonged exposure to noise that is above approximately 75-85 dB (Dowling, 2015).

The magnitude of how loud or intense a sound pressure wave is referred to as the amplitude of the wave. Sound amplitude is quantified using the decibel (dB) unit scale, which is derived from the base unit of the Pascal (Pa). The human ear is remarkably able to detect incredibly small sounds, with the human hearing threshold of hearing being approximately 20 millionths of a Pascal (Mahashabde, 2011). With the threshold of hearing being such a small value in the pascal scale, ordinary sound values gathered using the pascal scale will be very large and counterintuitive for practical measurements. For this reason, the sound pressure level (SPL) is often used to best equate the magnitude of a sound perceived by the human ear in decibels (Engineering ToolBox, 2004). The SPL equation can be seen in Equation 1. below where L_p is the sound pressure level in decibels, p is the sound pressure in pascals, and p_{ref} is the human threshold of hearing which is $2x10^{-5}$ pascals and acts as the reference sound pressure (Engineering ToolBox, 2004).

$$Lp = 20\log(p \div p_{ref})$$

Equation 1. Sound Pressure Level Equation

For this reason, the logarithmic decibel (dB) scale is used to compress the large range of the pascal scale into an intuitive scale to work with. In the decibel scale, the 20 uPa hearing threshold is used as the reference point to relate a given pascal value to its related decibel value. For example, when the pascal value is multiplied by ten, twenty is added to the decibel value. If the pascal value were to equal 200 uPa, the threshold value of 20 uPa (0 Db) would be referenced to show that the pascal value has been multiplied by ten. When the pascal value is multiplied by a value of ten, twenty is added to the decibel value thusly resulting in a value of 20 decibels for this example.

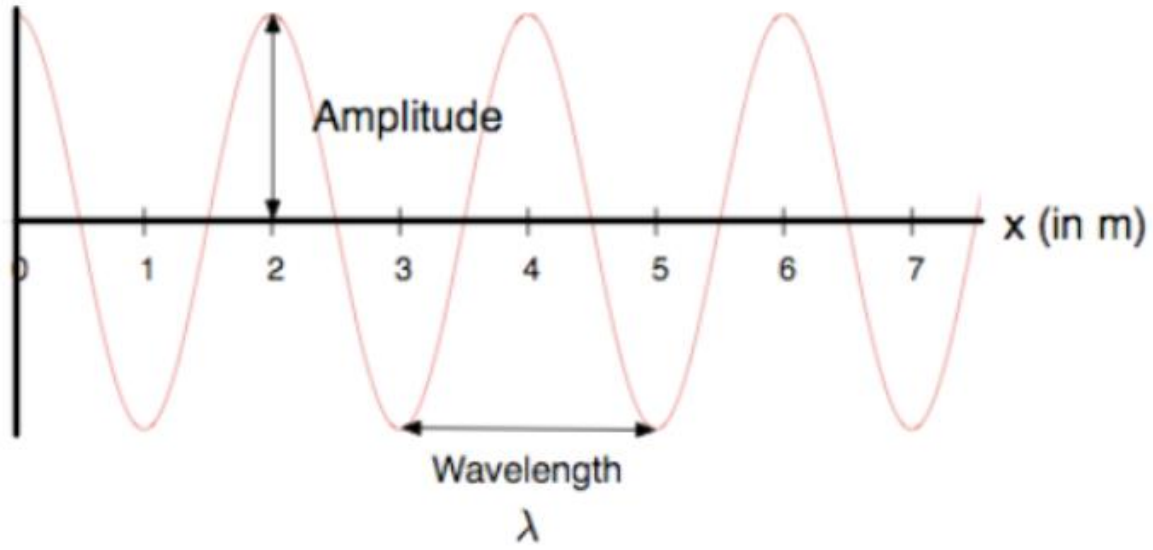

Figure 4: Waveform Key Components (Potter, 2020)

Another characteristic of a sound pressure wave to be considered is the wavelength, which is the distance from consecutive wave crests or wave troughs. The amount of time that passes during a single wavelength is referred to as the period of the wave and is inversely related to the frequency of the waveform (Measuring Sound, 1984).

$$\text{Wavelength } (\lambda) = \frac{Speed\ of\ Sound}{frequency}$$

Equation 2.0 Correlation Between Wavelength, Speed of Sound, and Frequency

A body is said to vibrate when it embodies oscillating motion about a reference point (Basner, 2014), and the number of oscillations or vibrations which occur in a second can be referred to as the frequency (Hz). While some vibrations occurring within a member are intended, most vibrations are generated from production imperfections or unbalanced forces occurring within the member. To view the full range of vibrations that occur within a given data set, it is required to view vibration signatures in the frequency spectrum.

Simple harmonic motion is the oscillation of a particle or point about a reference point and is sinusoidal by nature (Randall, 1987). While simple harmonic motion is useful in understanding the basics wave properties, such as the wavelength, period, fundamental frequency, and harmonic frequencies, most mechanical systems produce vibrations that are not simple sine waves. The more complex vibrations produced by turbojet engines for example can be better classified as non-harmonic periodic motion which is defined as an oscillation of a particle about a reference point in a non-uniform pattern (Randall, 1987). Since the non-uniform characteristics of non-harmonic motion make it impossible to define harmonics as simple harmonic motion would be evaluated, a method referred to as frequency analysis is applied.

Dating back to the early 1800's, Jean-Baptiste Joseph Fourier developed the number algorithm which is commonly known today as the Fourier Transform. Mathematicians such as Carl Friedrich Gauss, Cooley, and Tukey have made advancements to the Fourier Transform such that it is more compatible with the processing abilities of modern-day computers (Heideman, 1985). The most recent adaptation of the Fourier Transform is referred to as the Fast Fourier Transform (FFT) and is an efficient method to decompose a periodic signal into its respective sine waves.

2. Literature Review

2.1 Fuels

In the year 1923, Franz Fischer and Hans Tropsch developed a new method to create alternative fuels and named the method the Fischer-Tropsch Process. The FT process is a method in which many different carbon-based raw feedstocks such as coal, natural gas, and biomass can be synthesized into liquid and wax fuels (Hileman, 2009). The FT process removes large quantities of carbon dioxide (CO_2) from the feedstock chosen through a process stage referred to as gasification. After the CO_2 and other gases such as sulfur have been removed during gasification, the remaining synthesis gas is then passed over an iron or cobalt based catalyst forming a wide range of different hydrocarbons including gases and waxes (Hileman, 2009).

The FT process consists of three main stages which include the production of a synthesis gas from the feedstock, the removal of harmful gasses such as CO_2 from the concentrated synthesis-gas stream producing straight hydrocarbon chains, and the post processing of the straight hydrocarbon chains into more usable forms such as synthetic jet and automotive liquid fuels (Liu,

2013). As can be further evaluated in Figure 5. below, the feedstock coal can be converted into products such as automotive gasoline, diesels, and jet fuels such as Jet-A.

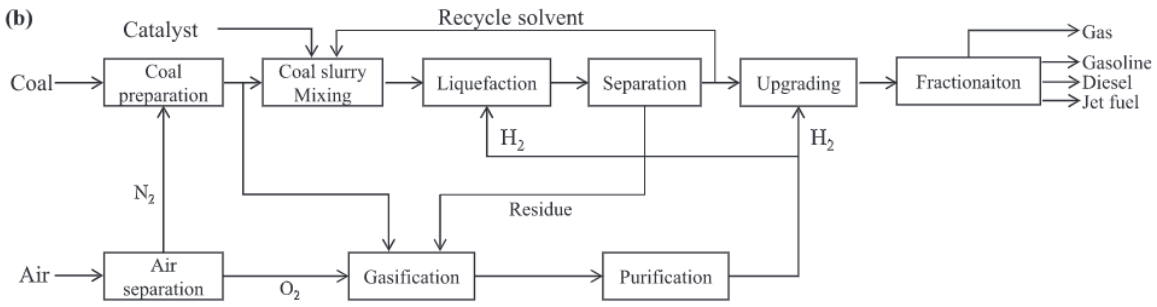

Figure 5. Fischer-Tropsch Synthesis of Coal to Liquid Petroleum (Ra, 2021)

Regarding the production of synthetic jet fuel, the Syntroleum Corporation has licensed a process in which they refer to as Bio-Synfining^{TM} in which feedstocks including vegetable oils, algae oils, fatty acids from animals, and greases can be converted to highly paraffinic fuels. In the Bio-Synfining^{TM}, the feedstock is first pretreated to remove materials such as water, metals, and phosphorous contaminants. From the pretreatment process, the fatty acid chains remaining are then converted to n-paraffins by exothermic hydrogenation and deoxygenation reactions in a hydrotreated. The last step of the Bio-Synfining^{TM} process includes the hydrocracking of the straight-chain paraffins into shorter branched paraffins (Liu, 2013).

Through the production process of creating gas to liquid SPK's, much of the aromatics which are necessary for enhancing fuel density and elastomer swelling properties are absent which can lead to major issues such as fuel line leaks (Selam, 2014). For this reason, SPK fuels are often blended with conventional aviation fuels to improve the aromatic requirements of the fuel to be

used in an aircraft. In a study conducted by Kai Chen et al., the sealant volume swell of materials such as polythioether and polysulfide used within aircraft fuel tanks and fuel lines was evaluated. In this study it was found that the swell of these materials dramatically increased as the aromatic content of the fuel increased, preventing the risk of leaking (Chen, 2013).

In a study performed by Matthew DeWitt et al., it was found that the presence of aromatics in fuels greatly impact the seal-swell capability within the fuel systems of aviation applications but also were found to increase engine soot emissions (DeWitt, 2008).

2.2 Emissions

As the World and specifically the United States are starting to take larger steps towards the reduction of greenhouse gas emissions, the transition from traditional fossil fuels to sustainable aviation fuels (SAF's) is becoming more commonplace. Jet A-1 is the conventional jet fuel of the aviation industry and is a kerosene-based fuel consisting of a mixture of thousands of hydrocarbons (Khandelwal, 2014). Traditional aviation fuels consist 20% of normal paraffins, 40% isoparaffins, 20% naphthenes, and 20% aromatics and Jet A in particular sets a maximum limit of aromatics to 25% to mitigate the risk of fuel leaks (Liu, 2013). Synthetic paraffinic kerosene (SPK's) such as S8 are a sustainable aviation fuel in which the feedstocks chosen are processed to remove contaminants, water, and 98% of the metal and phosphorous contaminants (Liu, 2013). The removal of these species leads to SPK's to have next to no aromatics in comparison to conventional aviation fuels leading to improved emissions characteristics.

When traditional aviation fuels such as Jet A are combusted, common emissions species produced include carbon dioxide, water vapor (H_2O), nitrogen oxides (NO_X), carbon monoxide (CO), and unburned hydrocarbons (UHC's) which are left to remain in the atmosphere (Riebl, 2017). One of the largest factors affecting the overall air quality is the emission of unburned

particulates into the atmosphere and sustainable aviation fuels in general produce less amounts of particulates they contain no fuel-bound nitrogen, sulfur, or aromatics (Riebl, 2017).

Water vapor is known to be Earth's most abundant greenhouse gas as carbon dioxide is one of the longest persisting greenhouse gases (Hansen, 2008). The white trails that follow aircraft in the skies are referred to as vapor contrails and consist of water vapor produced from the combustion process. The aircraft produced vapor contrails and the corresponding cirrus clouds formed by them substantially contribute to the aviation induced climate forcing (Kärcher, 2016). Vapor contrails typically come in three main variations, short-lived, persistent non-spreading, and persistent spreading contrails (NASA).

Until recently vapor contrails have not been investigated further than their existence, but recent satellite data has provided evidence of the heat-trapping effect which contrails have in the atmosphere (Hansen, 2008). According to NASA, recent data has reflected that as the surface temperatures continue to rise, so does the atmospheric humidity which forms a positive feedback loop (Hansen, 2008). As the global temperatures continue to rise from the introduction of more carbon dioxide gasses each year, more water vapor can be evaporated due to the higher temperatures, raising the atmospheric humidity. When water vapor is introduced into the cruising altitudes of airliners, the water vapor expands and collects thermal energy.

2.3 Noise and Vibrations

The terms sound and noise are often used interchangeably but this is a common misconception. Sound is best defined as a vibration which travels through air or another medium of interest whereas noise is better defined as unwanted or often damaging sound (Fink, 2019). The Environmental Protection Agency (EPA) has calculated that in order to prevent hearing loss, people should not exceed an average A-weighted sound magnitude of 70 decibels in a twenty-four-

hour time period (Fink, 2017). Other organizations such as the National Institute of Deafness and Other Communication Disorders have stated that decibel levels over 85 can lead to hearing loss and damage (Fink, 2017).

The human ear consists of three main components, the outer ear, the middle ear, and the inner ear. While the outer and middle ear might be more common to the average individual because these are the regions we can visually evaluate, the inner ear is the ear mechanism damaged by excessive noise levels. Within the inner ear is the cochlea which is a fluid filled body that captures the vibrations collected by the eardrum. Within the cochlea are many small auditory hairs known as inner and outer hair cells which collect the vibrations and pass the information to the brain by the auditory nerve (Hopkins, 2022). When an individual is exposed to excessive amounts of noise, the auditory hair cells within the cochlea are damaged and cannot be repaired which leads to permanent hearing loss.

In a study conducted by Tsan-Ju Chen et al., the hearing aptitude of a school near an airport including 228 students was compared to the hearing aptitude of a school located near an airport including 151 students. From the hearing tests performed on each group of students it was found that the students near the airport had a significantly worse hearing ability compared to the students located far away from the airport (Chen, 1993). Similar to the test performed by Chen et al., the noise exposure levels were measured for the crews of several different aircraft. In this research it was found that out of the different types of aircraft, the lowest measured cockpit A-weighted noise level was 85.5 decibels, and the maximum A-weighted noise level was 105.0 decibels (Gasaway, 1986). Both noise levels exceed the OSHA safety levels for sound exposure and justify further research into aircraft noise mitigation.

During the recent decades, the noise levels produced by the aviation industry has been reduced by approximately 20 Decibels (dB) (Khardi, 2008). The noise levels produced by an aircraft largely depend on the airframe-engine combination, but individual components such as the flaps, under-carriage, engine fan, or engine jet depending on what type of turbine-based engine is applied contribute largely to the overall noise level produced by an aircraft (Khardi, 2008).

Combustion noise and vibrations has become a topic of increasing interest as the aviation industry and technologies continue to advance. Because of advancements in aeroengines as of recent, many sound sources have been eliminated making combustion noise more prominent (Dowling, 2015). Another aspect to the growing interest in combustion noise and vibrations comes from the application of synthetic fuels to reduce the overall amount of greenhouse gases produced. While synthetic fuels are better from an emissions perspective on average, synthetic fuels commonly combust more unsteadily leading to increased amounts of combustion vibrations and noise (Dowling, 2015). While increased levels of vibrations and sound pressures are not always guaranteed to cause damage, it is ideal to limit these characteristics to mitigate component wear and fatigue. As was stated by Michael Cazalens, even if the acoustics activity does not produce damaging structural vibrations, the general noise level is usually regarded as unacceptable (Cazalens, 2008).

In a paper by Cumpsty, it was determined that the 400 Hz was an approximate peak frequency attributed to combustion within a turbine-based engine (Cumpsty, 1979). Within this research it was noted that because of the absence of fluctuating heat input in the combustion region, the combustion frequency between 400 and 500 Hz could not be precisely marked. Lastly in this research it was verified that the noise produced under 1,000 Hz was overwhelmingly generated by indirect combustion noise (Cumpsty, 1979). Direct and Indirect combustion noise co-exist within

the combustor of turbine engines where direct combustion noise is produced from unsteady combustion and indirect combustion noise is contributed by entropy fluctuations accelerating through components such as the exhaust nozzle (Tao, 2016). The direct combustion noise produced within a combustor has been observed to occur across the frequency range of 280 Hz to 500 Hz and remains relatively invariant regarding the operating conditions and burner geometry (Mathews, 1977).

3. Methodology

3.1 Single-Stage Gas Turbine Experimental Setup

A single-stage axial-flow turbojet gas turbine, which can be seen below in Figure 6., was applied for the testing in this paper. A turbojet variant of turbine-based engines produces 100% of its thrust from the expelling of hot combustion gasses through the exhaust nozzle of the engine. The key components focused upon in this research include the main turbojet shaft, the compressor, and the turbine of the engine. The turbine wheel of the turbojet engine captures the energy from the hot emissions gasses and turns this energy into an axial rotation. The turbine wheel is attached to the main shaft of the turbojet engine which translates the axial rotation of the turbine wheel to the compressor wheel located at the inlet of the engine. The compressor wheel of the turbojet engine pulls ambient pressure air from the inlet nozzle and compresses the air by a 3:1 ratio by the geometry of the compressor blades. The pressurized air from the compressor is then passed to the combustor of the engine where combustion occurs and is expelled out the internal exit nozzle (Turbine Technologies, 2011).

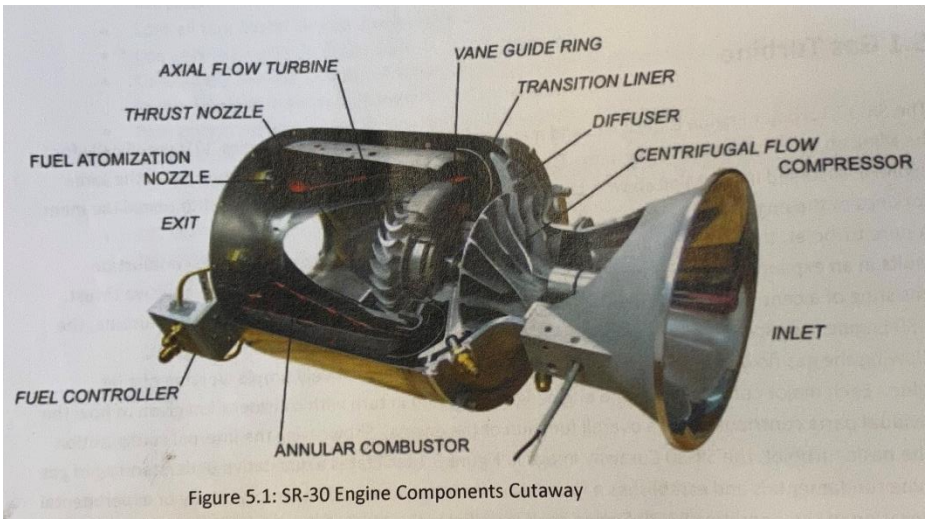

Figure 6. Single-Stage Turbojet Engine Main Components (Turbine Technologies, 2011)

The single-stage turbojet engine applied in this testing has a maximum thrust of 40 lbs. which is output at approximately 87,000 RPM. To collect data in a safe but repeatable environment, the single-stage turbojet engine was operated between the RPM range of 60,000 – 70,000 RPM taking data at 60,000 RPM, 65,000 RPM, and 70,000 RPM. Table 2. below includes both the theoretical maximum operating conditions in which the turbojet engine can operate along with the maximum conditions reached during testing.

	Maximum Conditions	Experimental Conditions
Maximum RPM	**87,000**	**70,000**
Maximum Inlet Temp. (°C)	**870**	**160**
Maximum Exhaust Temp. (°C)	**720**	**475**
Maximum Air Pressure (kPa)	**1,103**	**999**
Maximum Oil Pressure (kPa)	**70**	**138**
Maximum Ambient Temp. (°C)	**41**	**37**

Table 2. Single-Stage Turbojet Engine Maximum Operating Conditions (Turbine Technologies, 2011)

The single-stage turbojet engine applied in this research is instrumented with five pressure sensors (Setra Model 209) and K-type thermocouples which measure the pressures and temperatures at the inlet of the compressor, the exit of the compressor, the turbine inlet, the turbine exit, and lastly the exhaust nozzle. The before mentioned pressure and temperature monitoring positions can be better seen in Figure 7. below where the inlet nozzle is on the left and the exhaust nozzle on the right.

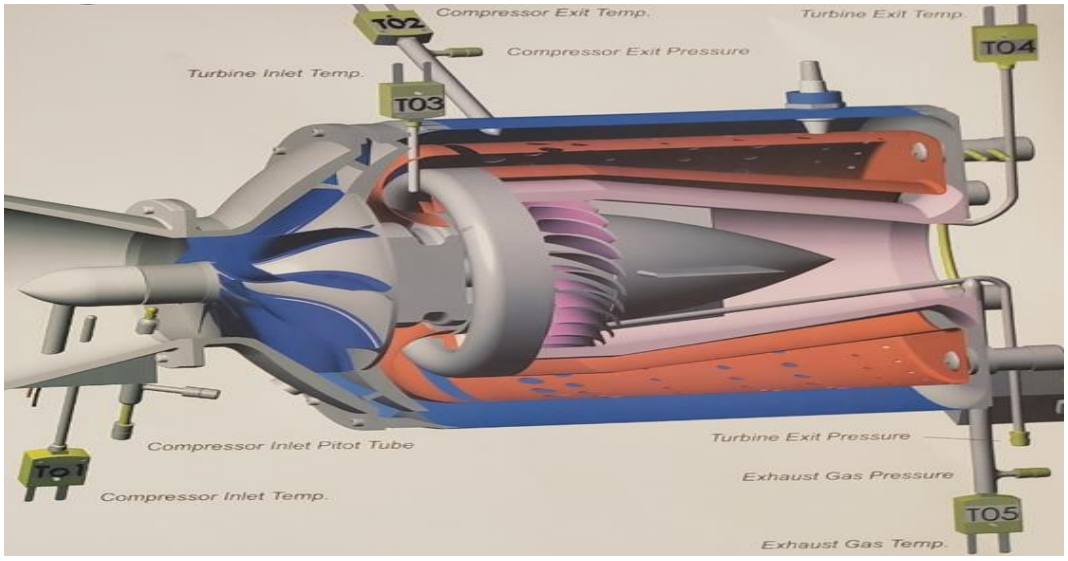

Figure 7. Experimental Pressure and Temperature Sensors Locations (Turbine Technologies, 2011)

Through the application of the Turbine Technologies MiniLab 1.2 Software, the data measured by the five Setra Model 209 pressure transducers and five K-type thermocouples can be evaluated live during testing and recorded for post experimentation processing. Along with the experimental pressures and temperatures recorded using the MiniLab 1.2 software, the thrust and operational speed of the turbojet engine are measured through the application of a load cell and tachometer respectively (Turbine Technologies, 2011). Through the live display of the MiniLab 1.2 software, a secondary form of monitoring the operational speed of the turbojet engine can be evaluated during experimentation along with the primary RPM being located on the main LCD screen of the turbojet engine experimental cabinetry. The presence of two operational speed displays allows for the safe operation of the turbojet engine to be monitored and maintained throughout the duration of experimentation. The five pressure transducer signals, K-type thermocouple signals, thrust values, and RPM values of the MiniLab 1.2 software can be evaluated below in Figure 8 below.

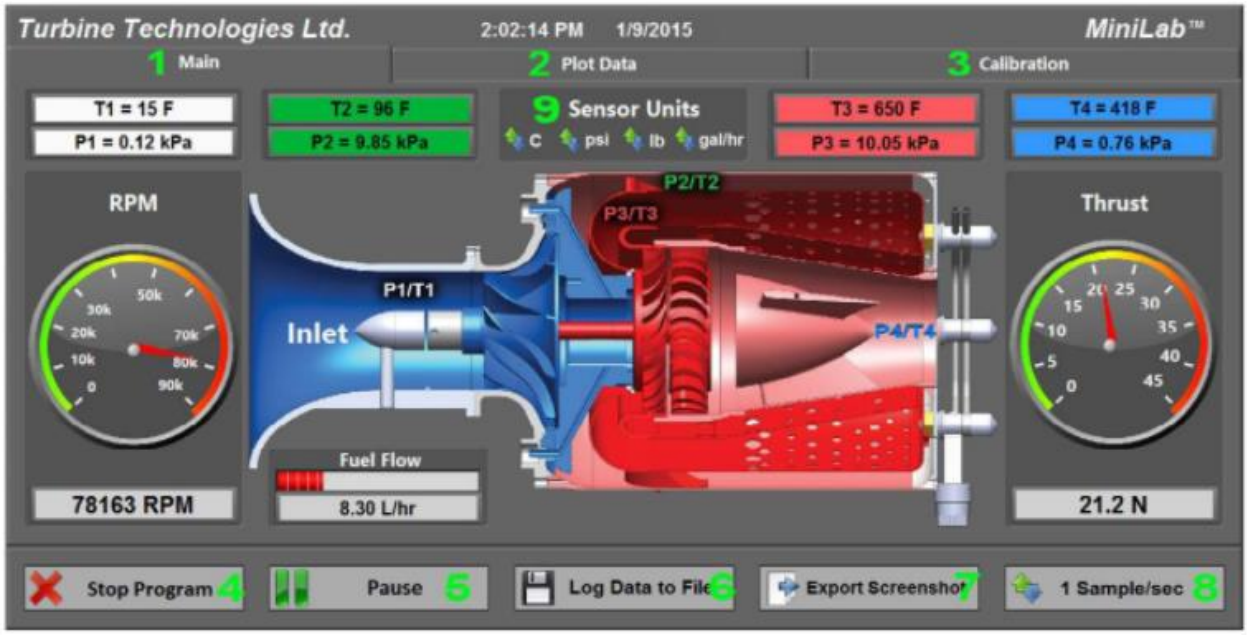

Figure 8. Turbine Technologies MiniLab 1.2 Software (Turbine Technologies, 2011)

3.2 Emissions

To analyze the emissions produced from the combustion of Jet A and S8 within the single-stage turbojet engine, a MKS MultiGas 2030 Fourier transform infrared spectroscopy (FTIR) analyzer was applied to the experimental setup. Through the passing of infrared radiation through the sample, the MKS FTIR can detect up to 25 different species of the exhaust gasses and particulates produced from combustion as seen in Table 3. below (MKS, 2017).

Name	Formula	Lowest Detectable Limit with 20/20™ Cell and 1 sec Measurement
Ammonia	NH_3	0.5 ppm
Carbon Dioxide	CO_2	0.2 ppm
Carbon Monoxide	CO	1.2 ppm
Formaldehyde	H_2CO	0.6 ppm
Hydrogen Chloride	HCl	1.5 ppm
Hydrofluoric Acid	HF	0.2 ppm
Methane	CH_4	0.6 ppm
Nitrogen Dioxide	NO_2	0.4 ppm
Nitric Oxide	NO	3.6 ppm
Nitrogen Trifluoride	NF_3	0.5 ppm
Silicon Tetrafluoride	SiF_4	0.15 ppm
Sulfur Dioxide	SO_2	0.6 ppm
Tetrafluoromethane	CF_4	40 ppb
Xylenes	C_8H_{10}	1.0 ppm

Table 3. MKS FTIR 2030 Emissions Species Detection Capability (MKS, 2017)

Due to the complex design of the MKS FTIR MultiGas™ 2030 Emissions Analyzer, the ambient environmental temperature and humidity have a large effect on measurement accuracy and overall safe operation of the emissions analyzer. Extreme temperatures and humidity levels surrounding the MKS FTIR MultiGas™ 2030 Emissions Analyzer can lead to the introduction of noise into the data signal up to electrical damage to the analyzer's internal components. The environmental temperature and humidity specifications of the MKS FTIR MultiGas™ 2030 Emissions Analyzer can be further evaluated in Table 4. and Table 5. below respectively.

	Temperature Range	Acceptable Variation
Acceptable Operating Range	10-32 °C	± 6 °C
	50-90 °F	± 11 °F
	Some signal loss to noise is acceptable	Loss of signal to noise, baseline drift noticeable
Optimal Operating Range	20-30 °C	± 3 °C
	68-86°F	± 5 °F
	Maximized Performance Range	No loss of performance, minimum baseline drift
Extreme Operating Range	5-38 °C	
	40-100 °F	
	Loss of signal to noise and electronics problems are possible	

Table 4. MKS FTIR MultiGas™ 2030 Emissions Analyzer Temperature Specifications

MKS MultiGas™ 2030 Humidity Specifications	
Optimal Operating Range	40%-60%
Extreme Operating Range	10%-80%

Table 5. MKS FTIR MultiGas™ 2030 Emissions Analyzer Humidity Specifications

Due to the narrow optimal operating range of the MKS emissions analyzer regarding both the temperature and humidity, the number of days of the year to perform tests are limited due to the on average high humidity levels seen in South Georgia. For this reason, the research conducted in this paper was limited to two full trials of Jet A and two full trials of S8.

3.3 Noise, Vibrations, and Harshness (NVH) Experimental Setup

To collect the sound pressures and vibrations produced by the combustion of Jet A and S8 in the single-stage turbojet engine, a combination of measurement microphones and a triaxial accelerometer were implemented into the test environment. To maintain repeatability and safe measurement techniques, the turbojet engine was positioned outdoors where the high temperature exhaust fumes could be safely dispersed into the ambient air during operation. The measurement of the sound pressures and vibrations outside also reflect realistic data to a full-scale turbojet operating in atmospheric conditions.

The two measurement microphones include a Bruel and Kjaer (HBK) Type 4944B ¼" Multifield Microphone and a Bruel and Kjaer Type 4966-H-041 ½" Freefield Microphone which were used in conjunction to collect the sound pressures produced by the operation of the turbojet engine. The Type 4944B ¼" Multifield Microphone is a Pressure-field class of microphone which specializes in high level and frequency measurements. The Type 4966-H-041 ½" Freefield Microphone because of its larger diameter and temperature rating allows for higher accuracy measurements outdoors and near operating machinery. The specifications of each microphone can be evaluated in Table 6. and Table 7. below.

Calibration Temperature	23 C
Ambient Static Pressure	101.3 kpa
Relative Humidity	50 %
Calibration Frequency	251.2 Hz
Polarization Voltage, external	0 V
Combined Sensitivity	-24.5 db re 1 V/Pa
Uncertainty 95% confidence level	0.3 db

Table 6. Type 4944B ¼" Multifield Microphone Specifications

Calibration Temperature	23 C
Ambient Static Pressure	101.3 kpa
Relative Humidity	50 %
Calibration Frequency	251.2 Hz
Polarization Voltage, external	0 V
Combined Sensitivity	-26.3 db re 1 V/Pa
Uncertainty 95% confidence level	0.2 db

Table 7. Type 4966-H-041 ½" Freefield Microphone Specifications

During experimentations, the Multifield and Freefield microphones were both fixed to tripods which were level with the midplane of the turbojet engine. The Multifield microphone was placed one meter directly perpendicular to the front face of the turbojet experimental cabinetry. The Freefield microphone was placed one meter from the exhaust outlet at a forty-five-degree angle so that the hot exhaust does not cause damage to the transducer. The placement of each microphone can be further evaluated in Figure 9. below.

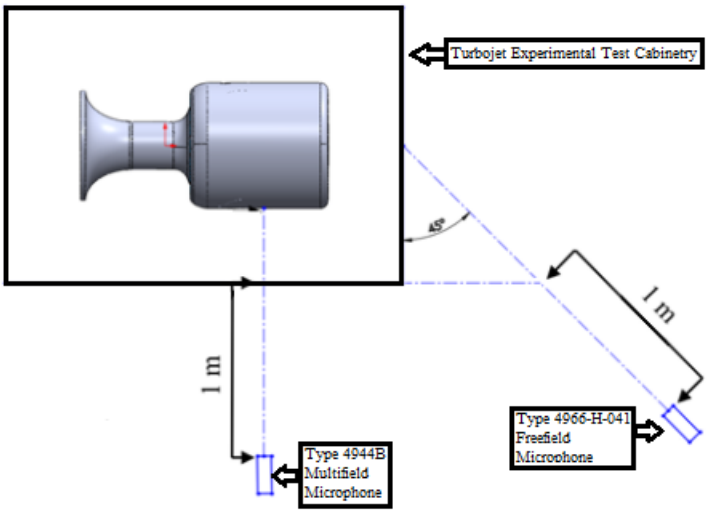

Figure 9. Experimental Microphone Setup

To collect the vibrations produced by the combustion of Jet A and S8 in the turbojet engine, a Bruel and Kjaer Triaxial DeltaTron® accelerometer was magnetically mounted to the engine mount of the experimental cabinetry. Due to the extreme temperatures and the turbojet being manufactured out of non-ferrous materials, the magnetic mount of the triaxial accelerometer must be mounted to the turbojet as seen in Figure 10. below. The placement of the triaxial accelerometer in this position was verified by the physical and environmental specifications of the Type 4527 triaxial accelerometer which can be seen in Table 8. and Table 9. below.

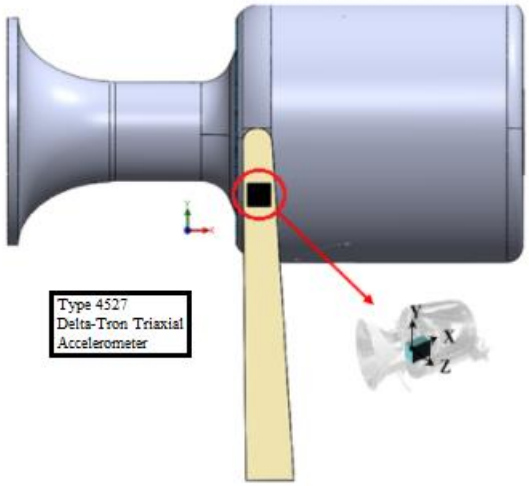

Figure 10. Triaxial Accelerometer Mounting Location and Orientation (Kilpatrick, 2019)

The triaxial accelerometer was placed such that the X-axis was parallel to the turbojet shaft, the Y-axis faced upwards towards the sky, and the Z-axis faced directly perpendicular to the mount face towards the operator. The triaxial accelerometer mounting location, X, Y, and Z axes can be seen above in Figure 10. In this orientation, the main vibrations produced by the radial motion of the turbojet main shaft, compressor wheel, and turbine wheel were accurately recorded.

	X	Y	Z
Reference Sensitivity	9.452 mv/g	9.939 mv/g	9.452 mvg
Frequency Range (Hz) : Amplitude (±10%)	0.3-10k[a] 0.3-5.5k[b]	0.3-10k[a] 0.3-5.5k[b]	0.3-12.8k[8]
Frequency Range (Hz): Phase (±5°)	2-10k[a] 2-5.5k[b]	2-10k[a] 2-5.5k[b]	2-12.8k[8]
Mounted Resonance Frequency (khz)	30[a] 19[b]	30[a] 17[b]	42[a]

Table 8. Type 4527 Triaxial DeltaTron® Accelerometer Physical Specifications

Environmental Temperature Range	-60° C to + 180°c (-76°f to +356°f)
Temperature Coefficient of Sensitivity	+0.12%/°c
Temp. Transient Sensitivity	0.02 ms^{-2}/°c
Magnetic Sensitivity	15 ms^{-2}/T
Base Strain Sensitivity	0.1 ms^{-2}/µ€
Max. Non-destructive shock	50 kms^{-2} peak (5100 g peak)

Table 9. Type 4527 Triaxial DeltaTron® Accelerometer Environmental Specifications

To evaluate the sound pressures and vibrations collected through the application of the Br*ü*el & Kjaer measurement microphones and triaxial accelerometer, a time domain Data Processing analysis was performed using the Br*ü*el & Kjaer software BK Connect 2019 edition (Hottinger, 2019). Through the application of the BK Connect 2019 software, the sound pressures and vibrations were recorded and post processed using filters such as the Constant

Percentage Bandwidth (CPB) for the sound pressures and the Fast Fourier Transform (FFT) for the vibration signatures. Through the application of the CPB and FFT filters, the sound pressures and vibrations signatures recorded with respect to time were translated to the frequency domain to perform a frequency analysis. After the CPB and FFT filters had been applied to the sound pressures and vibrations collected, the sound pressures correlated to combustion and vibrations correlated to the main turbojet shaft, compressor wheel, turbine wheel, and respective harmonics were evaluated. As can be further evaluated in Figure 11. and Figure 12. below, the Brüel & Kjaer software BK Connect 2019 edition is displayed.

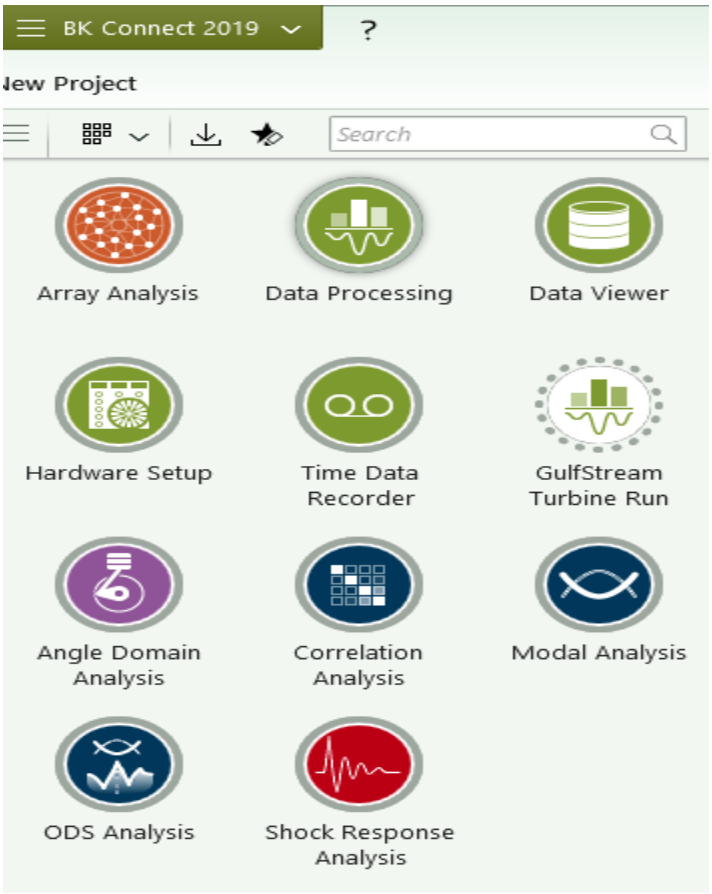

Figure 11. Brüel & Kjaer Software BK Connect 2019 Edition (Hottinger, 2019)

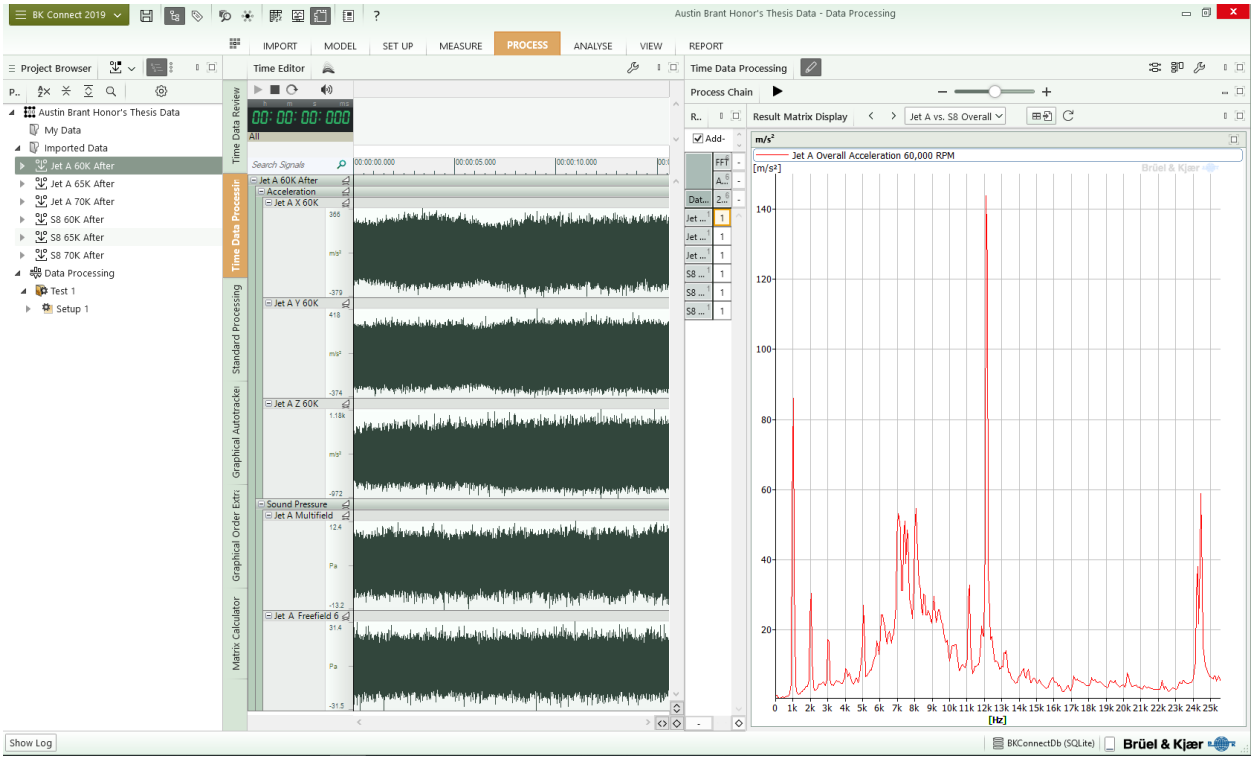

Figure 12. BK Connect 2019 Time Domain Analysis (Hottinger, 2019)

Experimental Machinery, Measurement Tools, and Software Setup

To collect the appropriate noise, vibrations, and emissions data necessary to evaluate the combustion differences between Jet A and S8, the following machinery, measurement tools, and software were required. The Turbine Technologies turbojet experimental cabinetry which includes five pressure and temperature sensors was connected to the Turbine Technologies software. The Turbine Technologies software displays and records the live pressure, temperature, and RPMs of the turbojet engine during operation (Turbine Technologies, 2011). The Type 4527 triaxial accelerometer was mounted to the engine mount of the turbojet experimental cabinetry and then connected to ports 1, 2, and 3 of the Bruel and Kjaer Type 3050-A-6/0 data acquisition board. Similarly, the Type 4944B Multifield and Type 4966-H-041 Freefield microphones were oriented

about the turbojet experimental cabinetry and then connected to ports 4 and 5 respectively of the Type 3050-A-6/0 data acquisition board. The Type 3050-A-6/0 data acquisition board was connected to the Bruel and Kjaer partnering software, BK Connect 2020, where the recorded combustion vibrations and sound pressures were processed using applications such as the Fast Fourier Transform (FFT) and the Constant Percentage Bandwidth (CPB) filters. A MKS MultiGas 2030 FTIR emissions analyzer was positioned such that the emissions species such as H_2O, CO, CO_2, NO_x, and other soot particulates produced by the combustion of Jet A and S8 could be evaluated. The experimental setup for the above-mentioned testing can be viewed in Figure 13. below.

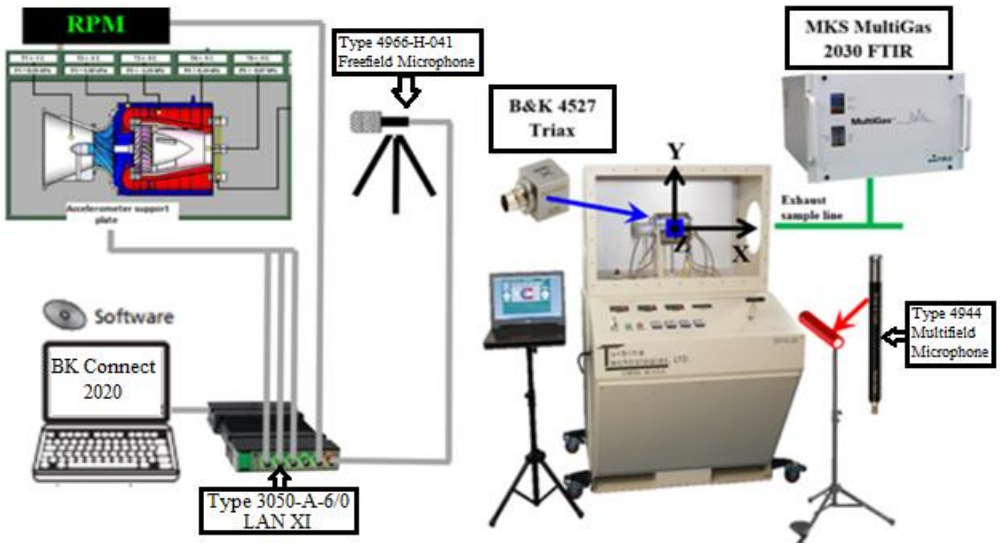

Figure 13. Turbojet Experimental Setup (Simons, 2016)

3.4 Experimental Procedure

To start the turbojet engine, a compressed air line of approximately 100 psi was attached to the turbojet experimental cabinetry to purge and spool the turbojet engine. After three main purging sequences were completed, to ensure that no contaminants were in the turbojet engine from storage, the turbojet was spooled until an idle speed of approximately 45,000 RPM was reached. From an idle, the turbojet was incrementally ramped upwards until the first test point at 60,000 RPM was reached. After waiting approximately 60 seconds to ensure that the RPM had stabilized at 60,000 RPM, the noise, vibrations, and emissions were recorded. After the recordings had been successfully saved, the turbojet operational speed was increased to 65,000 RPM and 70,000 RPM performing the same measurement techniques. After the recordings at 70,000 RPM had been completed, the turbojet operational speed was decreased to 65,000 RPM and 60,000 RPM taking additional recordings to aide in the creation of an average data. After the last recording at 60,000 RPM was completed, the turbojet engine was safely returned to an idle and then turned off.

For both Jet A and S8, two complete trials were performed to create an average set of noise, vibrations, emissions data at the turbojet operational speeds of 60,000 RPM, 65,000 RPM, and 70,000 RPM. A total of only four trials was largely limited by the specific temperature and humidity constraints of the MKS 2030 MultiGas FTIR emissions analyzer along with the safety-focused maintenance performed on the turbojet engine.

4. Results and Discussion

4.1 Vibrations Analysis

The vibrations signatures collected by the Type 4527 triaxial accelerometer included the vibrations in the X, Y, and Z directions which can be identified in Figure 8. above. To determine the overall vibrations produced by the combustion of each fuel, a vector sum was created from the X, Y, and Z directions of the triaxial accelerometer using the Matrix calculation function of BK Connect 2020. The vibrations in each axis were recorded over a frequency spectrum of 0 Hz to 26.6 kHz so that the vibrations of all components of the turbojet could be identified.

From the frequency analysis performed on the overall vibrations produced from the combustion of Jet A and S8 in the turbojet engine, key frequencies of interest included: the fundamental frequency produced from the main turbojet shaft rotation, the frequency produced by the twelve compressor blades, and lastly the frequency produced by the twenty-four turbine blades. The definition of a hertz is that one cycle occurs per second thus the fundamental frequency of the turbojet engine can be calculated by dividing the operating speed by 60. For example, the first test point at 60,000 RPM would have a fundamental frequency of 60,000 RPM divided by 60 equating to 1,000 Hz.

The turbojet is assembled where the compressor and turbine wheels are fixed upon the main turbojet shaft such that they rotate at the same speed as the shaft. With the compressor and turbine wheels rotating at the same speed as the main turbojet shaft, the frequency produced by each component will be equivalent to the fundamental frequency multiplied by the number of blades on each component. At 60,000 RPM for example, the frequency associated with the compressor wheel would equate to 1,000 Hz (The Fundamental Frequency) multiplied by the 12 compressor blades equaling 12,000 Hz. Table 10. below includes the key vibrations frequencies evaluated for both Jet A and S8 from 60,000 RPM to 70,000 RPM.

Component Frequencies (Hz)	60,000 RPM	65,000 RPM	70,000 RPM
Main Turbojet Shaft (Fundamental Frequency)	1,000	1,083	1,167
Compressor Wheel	12,000	12,996	14,004
Turbine Wheel	24,000	25,996	28,008

Table 10. Key Vibrations Frequencies

A critical portion of frequency analysis involves the differentiation between component-based frequencies as seen above in Table 10. and the respective harmonic frequencies of each component. The most prevalent harmonic frequencies identified through the operation of the turbojet engine include those of the main turbojet shaft rotation, which is also the fundamental frequency of the system. Harmonic frequencies by nature are multiples of the fundamental frequency and can be identified in this research as multiples of the 1,000 Hz fundamental frequency. As can be seen below in Figure 14. and Figure 15., the first, second, and third harmonics of the 1,000 Hz fundamental frequency can be evaluated using the BK Connect 2019 edition harmonics selector function. The first, second, and third harmonics occur at 2,000 Hz, 3,000 Hz,

and 4,000 Hz respectively and are identified as three diminishing amplitude peaks on the frequency spectrum.

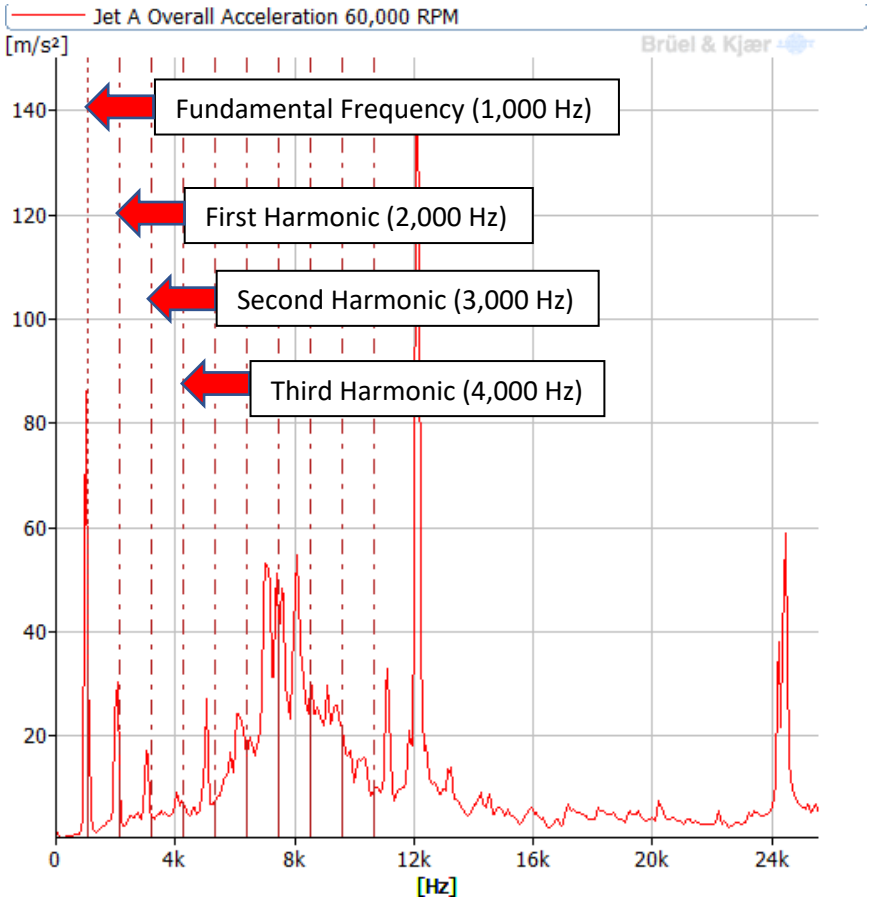

Figure 14. Fundamental and Harmonic Frequencies of Jet A (Hottinger, 2019)

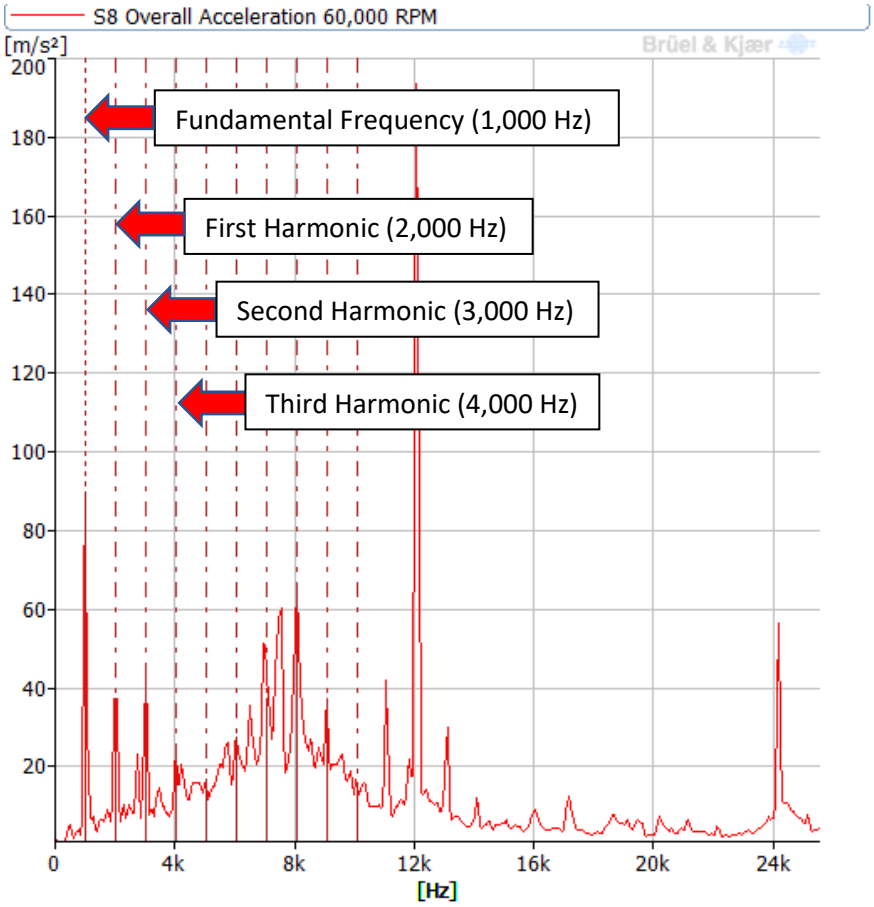

Figure 15. Fundamental and Harmonic Frequencies of S8 (Hottinger, 2019)

A frequency analysis has been performed as can be seen in Figures 16., 17., and 18. below, the overall accelerations of Jet A and S8 can be compared at 60,000 RPM, 65,000 RPM, and 70,000 RPM respectively. In each of the following three waveforms, Jet A is depicted in Red and S8 in Blue for ease of comparison and the entire frequency spectrum of 0 Hz to 25.6 kHz can be seen.

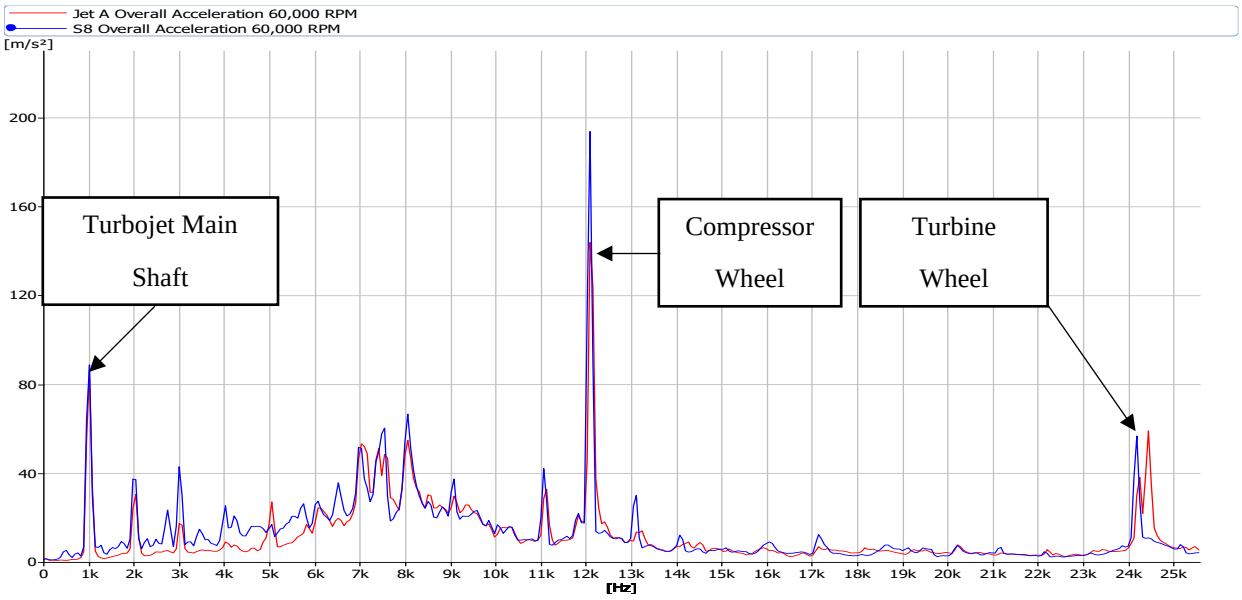

Figure 16. Overall Acceleration comparison of Jet A and S8 at 60,000 RPM

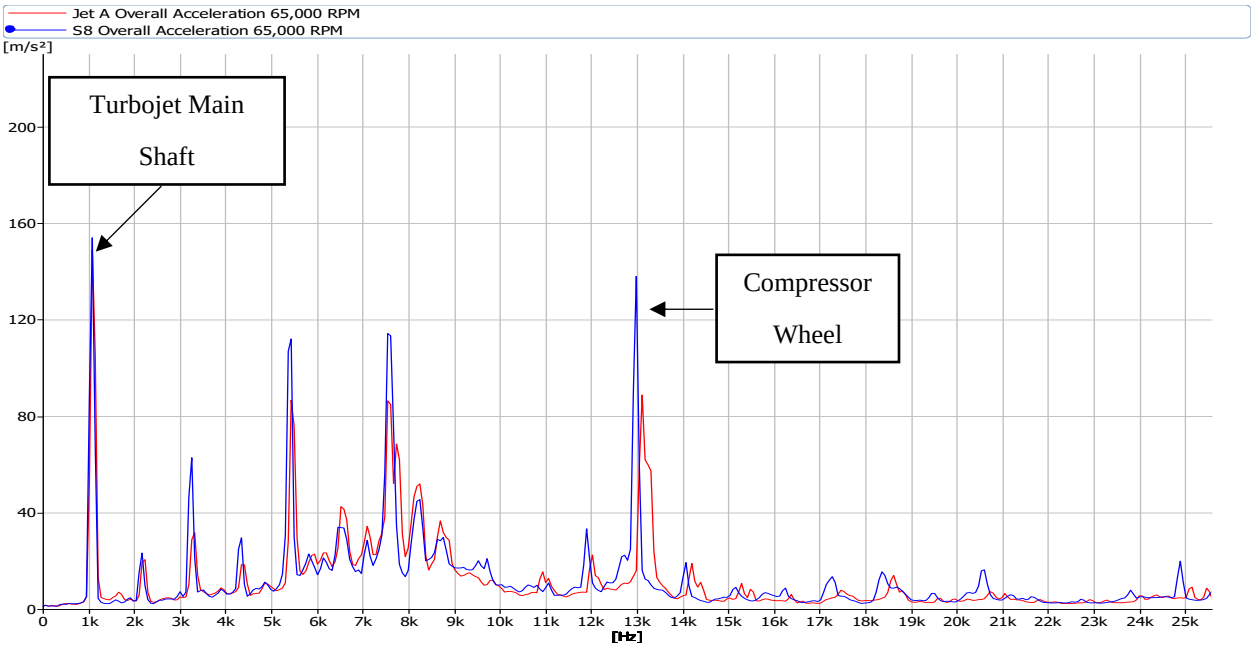

Figure 17. Overall Acceleration comparison of Jet A and S8 at 65,000 RPM

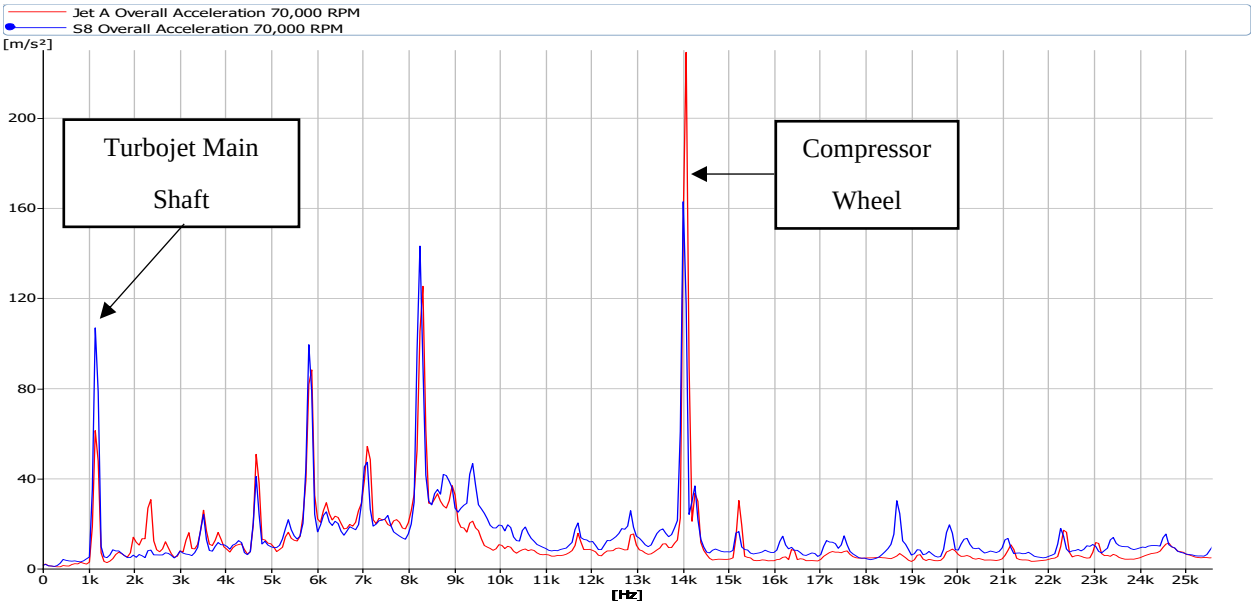

Figure 18. Overall Acceleration comparison of Jet A and S8 at 70,000 RPM

As can be seen in Figures 16. through Figure 18. above, S8 on average produced greater magnitudes of acceleration compared to Jet A across the frequency spectrum of 0 Hz to 25.6 kHz. As can be evaluated in Table 11. Below, the greatest magnitude of vibrations produced by the main turbojet shaft occurred at 65,000 RPM where S8 produced 193.66 m/s^2 of acceleration and Jet A produced 148.72 m/s^2 of acceleration. The acceleration of the main turbojet shaft at 65,000 is approximately 100% greater than the accelerations produced at 60,000 RPM and 70,000 RPM and can be potentially explained as a near critical speed of the turbojet shaft.

The greatest magnitudes of vibrations produced by the compressor wheel occurred at 70,000 RPM where Jet A produced 229.05 m/s^2 of acceleration and S8 produced 162.76 m/s^2 of acceleration. Because of the high frequency emitted by the rotation of the turbine wheel of the turbojet engine, the vibrations produced by the turbine wheel could only be recorded at 60,000 RPM before exceeding the frequency range applied during experimentation. The overall levels of vibrations produced by the turbine wheel at 60,000 RPM were marginal compared to the main turbojet shaft and compressor wheel but consisted of 58.97 m/s^2 of acceleration for Jet A and 56.67 m/s^2 of acceleration for S8.

Component Acceleration (m/s^2)	60,000 RPM		65,000 RPM		70,000 RPM	
	Jet A	S8	Jet A	S8	Jet A	S8
Main Turbojet Shaft	86.17	88.66	148.72	193.66	61.21	56.67
Compressor Wheel	143.74	193.66	88.7	137.88	229.05	162.76
Turbine Wheel	58.97	56.67	Na.	Na.	Na.	Na.

Table 11. Key Turbojet Components Magnitudes of Acceleration

4.2 Sound Pressure Analysis

The sound pressures recorded using the Type 4944B Multifield and Type 4966-H-041 Freefield microphones were recorded across a frequency spectrum of 0 Hz to 16 kHz. Because the Decibel scale is logarithmic in nature, the X-axis of Figures 19. through 21. below is likewise set in a logarithmic scale to best represent the acoustic signatures recorded. The Multifield and Freefield microphones displayed near identical sound pressure values across the frequency spectrum but because of the design specifications of the Freefield microphone to be used outdoors primarily, the sound pressures collected by the Freefield microphone were further evaluated.

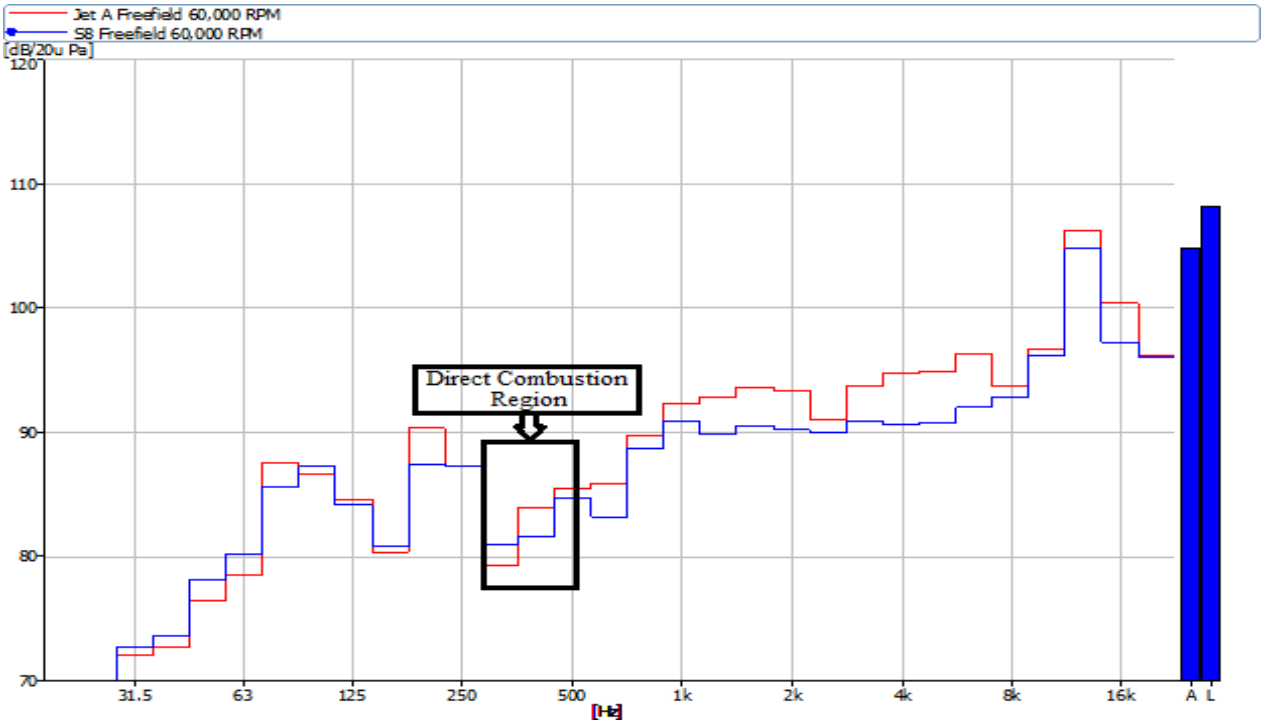

Figure 19. Freefield Sound Pressure Comparison between Jet A and S8 60,000 RPM

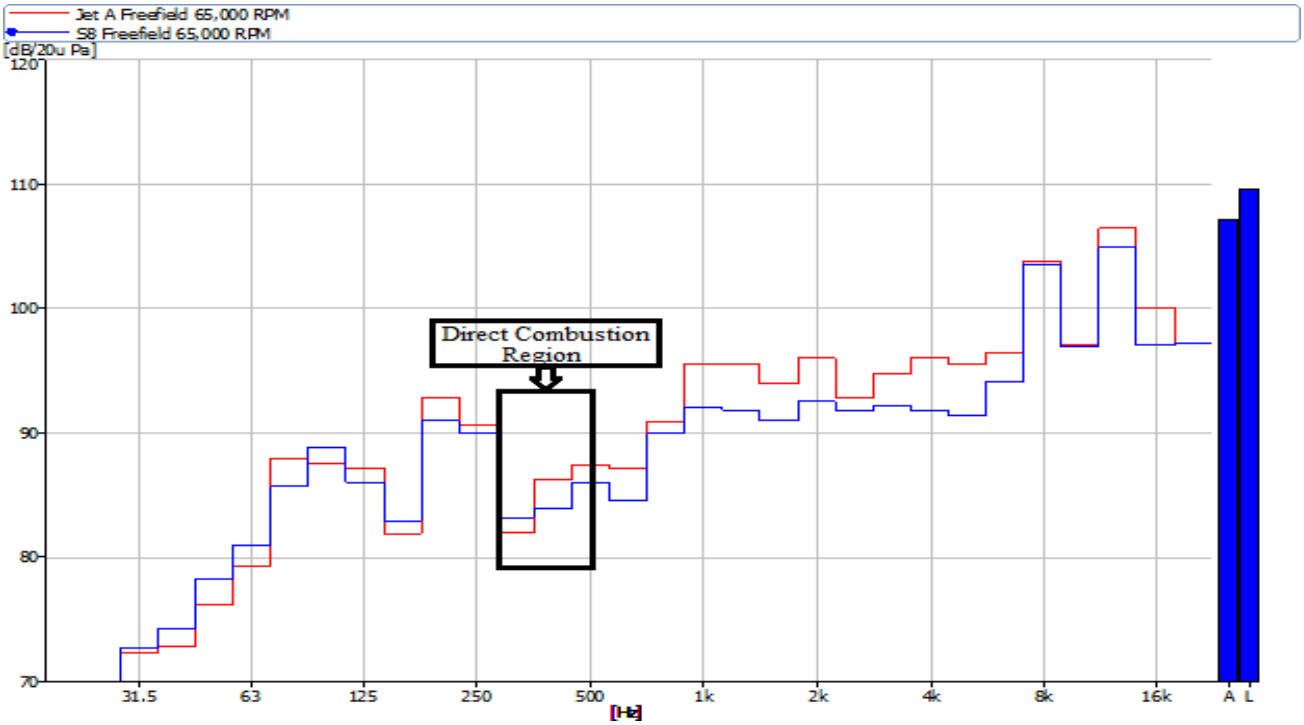

Figure 20. Freefield Sound Pressure Comparison between Jet A and S8 65,000 RPM

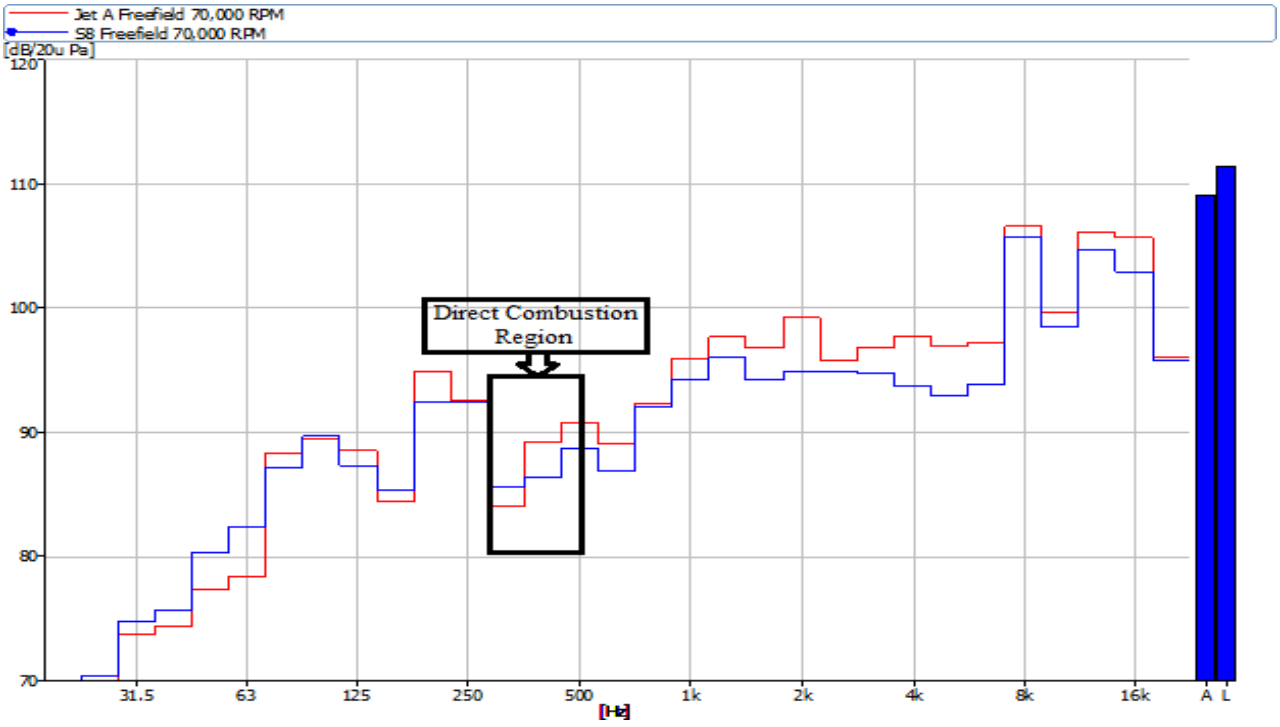

Figure 21. Freefield Sound Pressure Comparison between Jet A and S8 70,000 RPM

As can be seen in Figures 19. through 21. above, an overall increasing trend in sound pressure magnitude can be evaluated as the upper limit of the 0 Hz to 16 kHz frequency range was reached with the peak sound pressures produced by each fuel occurring at 12,500 Hz. The peak sound pressure produced by Jet A and S8 at 70,000 RPM and 12,500 Hz were 106.6 dB and 104.73 dB respectively. On average Jet A produced greater magnitudes of sound pressures across the entire frequency spectrum when compared to S8. At approximately 300 Hz for each of the three test points, S8 produced greater magnitudes of sound pressure when compared to Jet A and this region can be attributed to the combustion process of each fuel.

In Figures 19. through 21. above, the direct combustion noise produced from unsteady combustion can be evaluated across the frequency range of approximately 280 Hz to 500 Hz. From the noise signatures collected at 60,000 RPM, 65,000 RPM, and 70,000 RPM, it was found that S8 produced greater magnitudes of sound pressure from 280 Hz to 375 Hz of the direct combustion noise region (280 – 500 Hz) and Jet A produced greater magnitudes of sound pressure 375 Hz to 500 Hz of the direct combustion noise region. This can be explained by the natural tendency of synthetic fuels such as S8 to burn more unsteady in relation to conventional fuels such as Jet A.

4.3 Emissions Analysis

The emissions results for percentage water vapor (H_2O), the percentage carbon dioxide (CO_2), and parts per million of unburned hydrocarbons (THC) produced during the combustion of Jet A and S8 can be seen in Figure 22. through Figure 24. respectively. The parts per million carbon monoxide (CO) and parts per million nitrous oxides (NO_X) can be evaluated in relation to the H_2O%, CO_2%, and parts per million of THC at 70,000 RPM in Table 12. below. The above-mentioned emissions species produced by each fuel were compared by the individual emissions

species at 60,000 RPM, 65,000 RPM, and 70,000 RPM so that the optimal operating speed of the turbojet could be determined. While S8 on average produced less emissions overall when compared to Jet A across the test points 60,000RPM, 65,000RPM, and 70,000RPM, the greatest emissions difference between Jet A and S8 can be seen in the overall amount of water vapor and un-burnt hydrocarbons emitted.

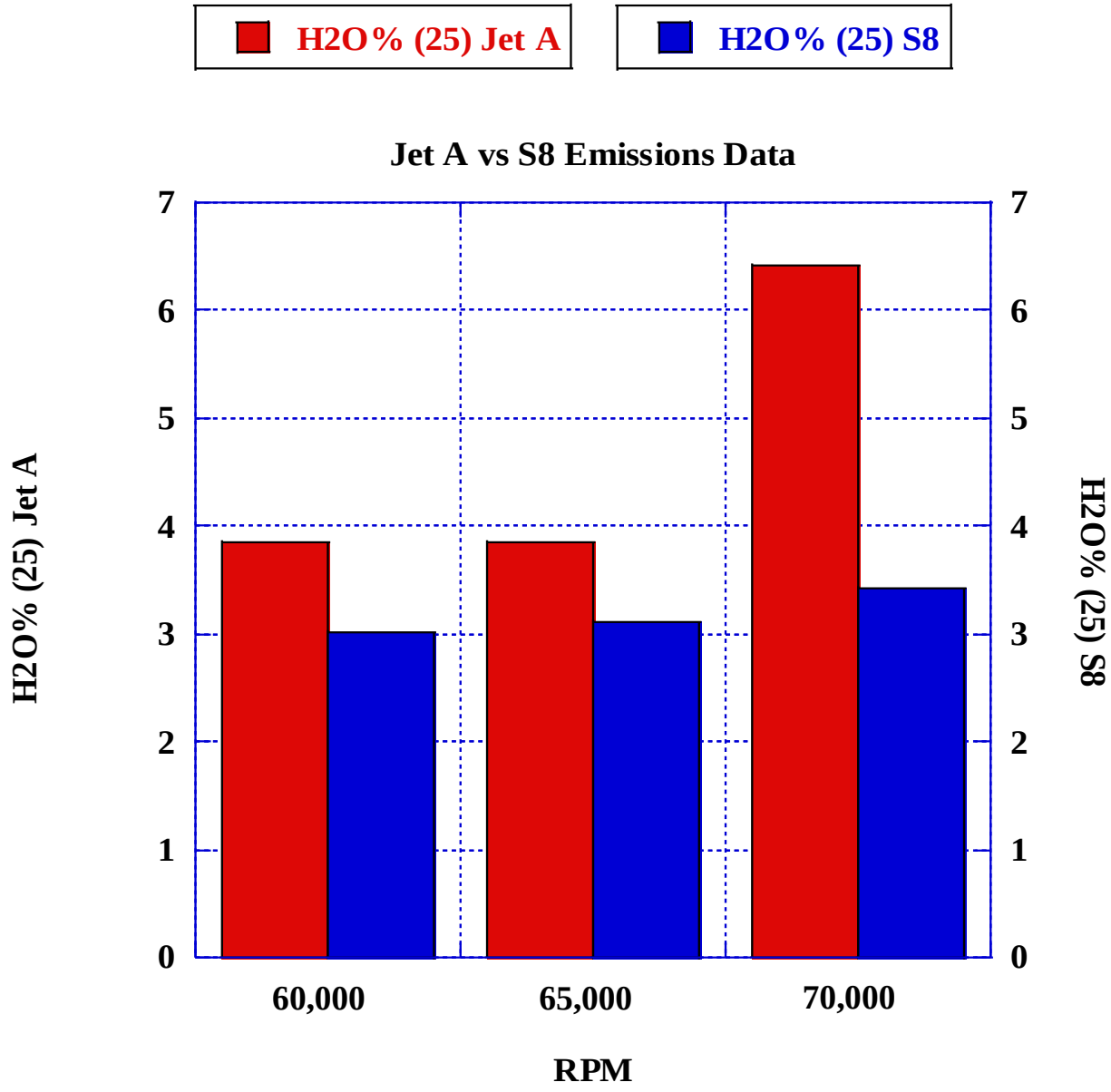

Figure 22. H_2O Vapor Emissions Percentage per RPM

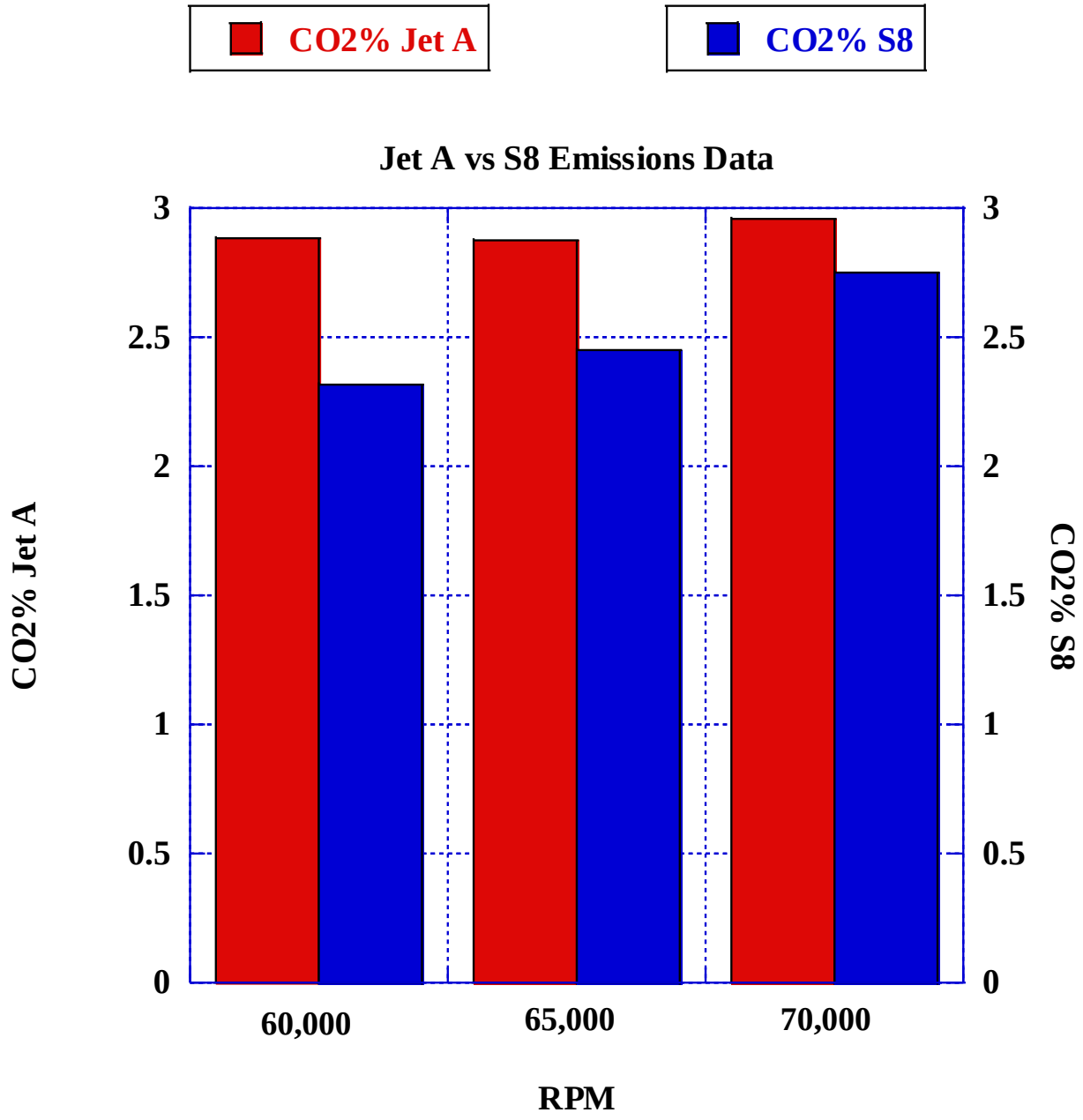

Figure 23. CO_2 Emissions Percentage per RPM

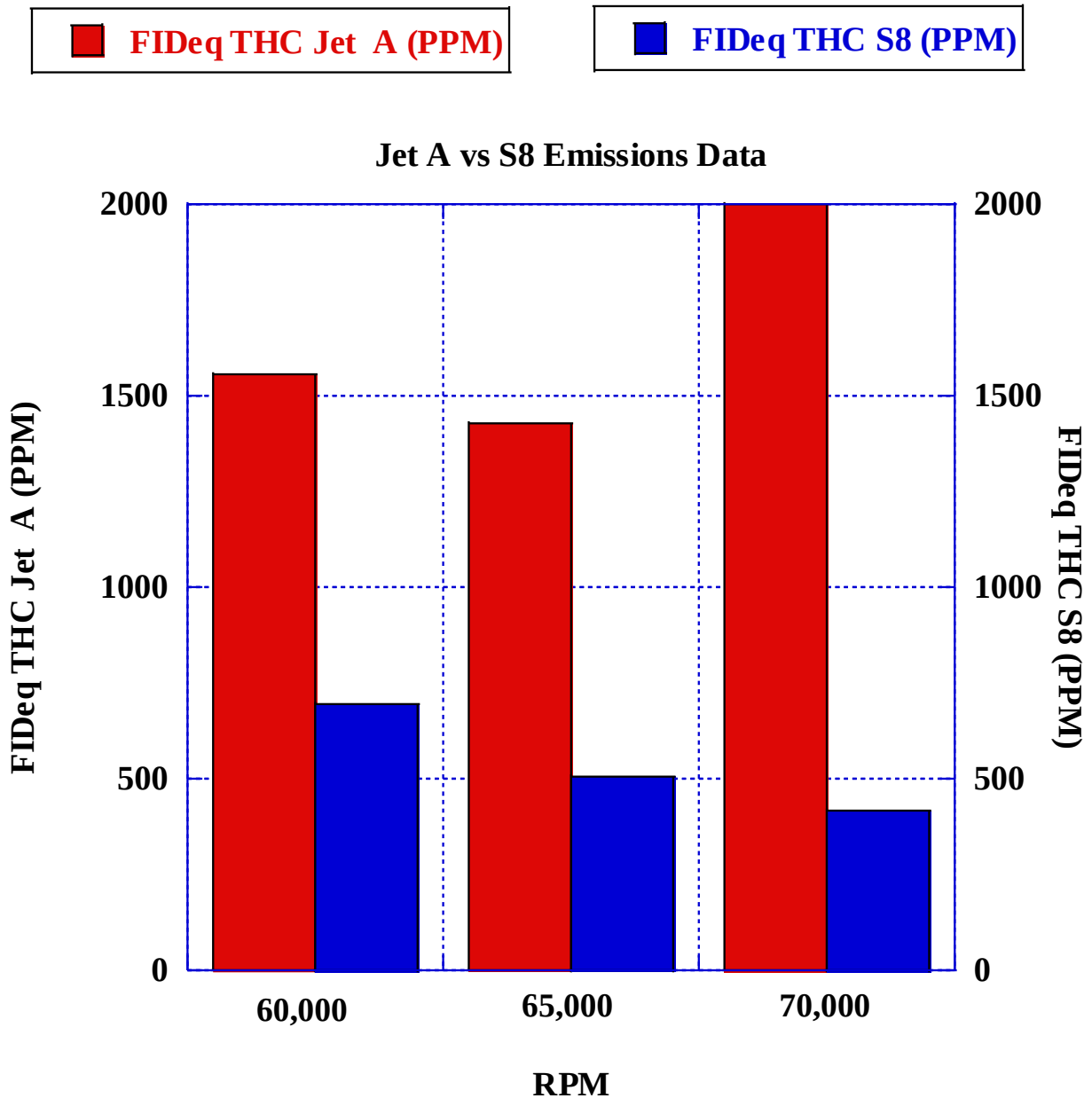

Figure 24. Soot Emissions Parts per Million per RPM

As can be seen in Figure 22 above, S8 produced .9% less water vapor at 60,000 RPM, .8% less water vapor at 65,000 RPM, and 3% less water vapor at 70,000 RPM. The maximum percentage of water vapor produced by each fuel occurred at 70,000 RPM where Jet A produced 6.5% water vapor at 70,000 RPM and S8 produced 3.5% water vapor at 70,000 RPM. The overall reduction in water vapor emissions produced by the combustion of S8 can be explained by the Bio-Synfining^{TM} process in which the water composition and other particulates are completely removed from the feedstocks applied in S8 production.

On average, S8 produced less carbon dioxide gas than Jet A at all three test points but in specific produced .5% less CO_2 at 60,000 RPM, .35% CO_2 at 65,000 RPM, and .15% CO_2 at 70,000 RPM. The maximum about of carbon dioxide emitted occurred at 70,000 RPM for each fuel where Jet A and S8 produced 2.9% and 2.75% CO_2 respectively. Regarding the quantity of unburned hydrocarbons emitted by each fuel, S8 produced 900 ppm less unburned hydrocarbons than Jet A at 60,000 RPM, 900 ppm less than Jet A at 65,000 RPM, and 1,600 ppm less than Jet A at 70,000 RPM. The maximum number of unburned hydrocarbons produced by Jet A occurred at 70,000 RPM where 2,000 ppm were emitted while S8 produced a maximum of 650 ppm at 60,000 RPM.

Because S8 progressively produces less unburned hydrocarbons as the operational speed of the turbojet engine was increased from 60,000 to 70,000 RPM, it was determined that S8 combusted most efficiently at 70,000 RPM in comparison to the conventional fuel Jet A. This claim was also verified by the maximum water vapor percentage produced occurring at 70,000 RPM which is an indicator of complete combustion. In Table 10. below, the percentage differences in water vapor, carbon dioxide, and unburnt hydrocarbon emissions between Jet A and S8 can be seen.

Because 70,000 RPM on average consisted of the most efficient combustion, the combustion species produced by Jet A and S8 were further compared to create a percentage difference as can be seen in Table 12. below. At 70,000 RPM it was found that S8 produced 61.22% less water vapor than Jet A, 5.31% less carbon dioxide emissions, 18.18% less carbon monoxide emissions, 3.64% less nitrous oxide emissions, and lastly 133.33% less unburned hydrocarbons than Jet A. From the net positive percentages in the emissions produced by S8 in comparison to Jet A, it was determined that S8 combusted more efficiently and cleanly than Jet A at 70,000 RPM.

Emissions Species	Jet A	S8	% Difference Between Jet A and S8
H_2O (%)	6.4	3.4	61.22 %
CO_2 (%)	2.9	2.75	5.31 %
CO (PPM)	1,050	875	18.18 %
NO_x (PPM)	28	27	3.64 %
THC (PPM)	2,000	400	133.33 %

Table 12. Jet A and S8 Combustion Emissions at each Operational Speed (RPM)

5. Conclusions

From the evaluation of the sound pressures, vibrations, and emissions produced by the combustion of Jet A and S8 within the single-stage turbojet engine, it has been proven that the optimal operating speed of the turbojet engine is 70,000 RPM. The maximum magnitude of vibrations produced by the main turbojet shaft rotation occurred at 65,000 RPM and was 193.66 m/s^2 by Jet A. The maximum magnitude of vibrations produced by the compressor wheel occurred at 70,000 RPM and was 229.05 m/s^2 by Jet A. The maximum magnitude of vibrations produced by the turbine wheel at 65,000 RPM and 70,000 RPM exceeded the upper limit of the frequency

range applied during experimentation but can be assumed to be in close relation to the magnitudes 58.97 m/s^2 and 56.67 m/s^2 produced by Jet A and S8 respectively at 60,000 RPM.

Similar to the vibration signatures collected from the combustion of Jet A and S8 in the turbojet engine, the sound pressures recorded remain relatively consistent across all three operational speeds with 70,000 RPM producing the largest magnitudes of sound pressure. The greatest magnitude of sound pressures recorded at each operational speed occurred at a frequency of approximately 12,500 Hz with 70,000 RPM producing a peak sound pressure of 106.6 dB and 104.73 dB for Jet A and S8 respectively. The peak sound pressures produced by Jet A and S8 at 70,000 RPM can be potentially correlated to the extreme air flows occurring within the turbojet assembly as it operates at high velocities.

From the emissions signatures collected at each operating speed, it was proven that the most emissions efficient operating speed was 70,000 RPM in which S8 produced 61.22% less water vapor, 5.31% less carbon dioxide gas, 18.18% less carbon monoxide emissions, 3.64% less nitrous oxide emissions, and lastly 133.33% less unburned hydrocarbons than Jet A. The mitigation of the before mentioned emissions species through the application of S8 allows for vapor contrail production to be minimized along with improving air quality.

Future research that could be explored would be the blending of conventional fuels such as Jet A with Sustainable Aviation Fuels (SAF's) such as S8 so that the aromatics required of an airline grade fuel could be met. Through the testing of a new conventional-synthetic fuel, emissions testing could be performed to evaluate if the excessive amounts of water vapor produced from the combustion of Jet A could be mitigated to prevent the likeliness of vapor contrail production. Similarly, the vibrations and sound pressures produced by the newly blended fuel could be evaluated to see if a possibly quieter operating fuel could be discovered.

6. References

Barnett, Jessee. “Demand for Jet Fuel in the U.S. Is Recovering Faster than in Many Other Markets.” Demand for jet fuel in the U.S. is recovering faster than in many other markets - Today in Energy - U.S. Energy Information Administration (EIA), 2020. https://www.eia.gov/todayinenergy/detail.php?id=44996#:~:text=EIA%20estimates%20that%20as%20of,same%20date%20one%20year%20earlier.

Basner, Mathias, Wolfgang Babisch, Adrian Davis, Mark Brink, Charlotte Clark, Sabine Janssen, and Stephen Stansfeld. “Auditory and Non-Auditory Effects of Noise on Health.” *The Lancet* 383, no. 9925 (2014): 1325–32. https://doi.org/10.1016/s0140-6736(13)61613-x.

Blakey, Simon, Lucas Rye, and Christopher Willam Wilson. “Aviation Gas Turbine Alternative Fuels: A Review.” *Proceedings of the Combustion Institute* 33, no. 2 (2011): 2863–85. https://doi.org/10.1016/j.proci.2010.09.011.

Buis, Alan. “Steamy Relationships: How Atmospheric Water Vapor Supercharges Earth's Greenhouse Effect – Climate Change: Vital Signs of the Planet.” NASA. NASA, February 8, 2022. https://climate.nasa.gov/ask-nasa-climate/3143/steamy-relationships-how-atmospheric-water-vapor-supercharges-earths-greenhouse-effect/.

Cazalens, Michel, Sébastien Roux, Claude Sensiau, and Thierry Poinsot. “Combustion Instability Problems Analysis for High-Pressure Jet Engine Cores.” *Journal of Propulsion and Power* 24, no. 4 (2008): 770–78. https://doi.org/10.2514/1.30938.

Chen, Kai, Hua Liu, and Zuxi xia. “The Impacts of Aromatic Contents in Aviation Jet Fuel on the Volume Swell of the Aircraft Fuel Tank Sealants.” *SAE International Journal of Aerospace* 6, no. 1 (2013): 350–54. https://doi.org/10.4271/2013-01-9001.

Chen, Tsan-Ju, and Shun-Sheng Chen. “Effects of Aircraft Noise on Hearing and Auditory Pathway Function of School-Age Children.” *International Archives of Occupational and Environmental Health* 65, no. 2 (1993): 107–11. https://doi.org/10.1007/bf00405728.

Cumpsty, N.A., Jet Engine Combustion Noise: Pressure, Entropy and Vorticity Perturbations produced by Unsteady Combustion or Heat Addition (Cambridge, England: Department of Engineering, Cambridge University, 1979). https://doi.org/10.1016/0022-460X(79)90697-7

DeWitt, Matthew J., Edwin Corporan, John Graham, and Donald Minus. “Effects of Aromatic Type and Concentration in Fischer−Tropsch Fuel on Emissions Production and Material Compatibility.” *Energy & Fuels* 22, no. 4 (2008): 2411–18. https://doi.org/10.1021/ef8001179.

Dowling, Ann P., and Yasser Mahmoudi. “Combustion Noise.” *Proceedings of the Combustion Institute* 35, no. 1 (2015): 65–100. https://doi.org/10.1016/j.proci.2014.08.016.

Edwards, James T. *Jet Fuel Properties*. Air Force Research Laboratory Wright-Patterson AFB United States, 2020.

Engineering ToolBox, (2004). *Sound Pressure.* Accessed 3 31, 2022. Available at: https://www.engineeringtoolbox.com/sound-pressure-d_711.html [Accessed Day Mo. Year].

Fink, Daniel J. "What Is a Safe Noise Level for the Public?" *American Journal of Public Health* 107, no. 1 (2017): 44–45. https://doi.org/10.2105/ajph.2016.303527.

Fink, Daniel. "A New Definition of Noise: Noise Is Unwanted and/or Harmful Sound. Noise Is the New 'Secondhand Smoke'." *Proceedings of Meetings on Acoustics*, 2019. https://doi.org/10.1121/2.0001186.

Gasaway, Donald C. "Noise levels in cockpits of aircraft during normal cruise and considerations of auditory risk." *Aviation, space, and environmental medicine* 57, no. 2 (1986): 103-112.

Hansen, Kathryn. "Water Vapor Confirmed as Major Player in Climate Change." NASA. NASA, 2008. https://www.nasa.gov/topics/earth/features/vapor_warming.html?msclkid=046bdf97a98211ec9c7e5a431d612b38.

Heideman, Michael T., Don H. Johnson, and C. Sidney Burrus. "Gauss and the History of the Fast Fourier Transform." *Archive for History of Exact Sciences* 34, no. 3 (1985): 265–77. https://doi.org/10.1007/bf00348431.

Hileman, James, Ortiz David, Bartis James, Wong Hsin et al. Near-Term Feasibility of Alternative Jet Fuels. RAND Corporation, 2009. https://rosap.ntl.bts.gov/view/dot/18417

Hopkins, Johns. "How the Ear Works." Johns Hopkins Medicine. The Johns Hopkins University, 2022. https://www.hopkinsmedicine.org/health/conditions-and-diseases/how-the-ear-works.

Hottinger Brüel & Kjær, BK Connect (2019). Version Number 23.0.0.935. Brüel & Kjær Sound & Vibration Measurement A/S, 2020.

HOWE, M. S. "Indirect Combustion Noise." *Journal of Fluid Mechanics* 659 (2010): 267–88. https://doi.org/10.1017/s0022112010002466.

Huq, Nabila A., Glenn R. Hafenstine, Xiangchen Huo, Hannah Nguyen, Stephen M. Tifft, Davis R. Conklin, Daniela Stück, et al. "Toward Net-Zero Sustainable Aviation Fuel with Wet Waste–Derived Volatile Fatty Acids." *Proceedings of the National Academy of Sciences* 118, no. 13 (2021). https://doi.org/10.1073/pnas.2023008118.

Khandelwal, Bhupendra, Swapneel Roy, Charles Lord, and Simon Blakey. "Comparison of Vibrations and Emissions of Conventional Jet Fuel with Stressed 100% SPK and Fully

Formulated Synthetic Jet Fuel." *Aerospace* 1, no. 2 (2014): 52–66. https://doi.org/10.3390/aerospace1020052.

Khardi, S. (2008). An Experimental Analysis of Frequency Emisison and Noise Diagnosis of Commercial Aircraft on Approach. J. Acoustic Emission, 26, 290- 310.

Kilpatrick, M. (2019). The Investigation of Noise, Vibrations, and Emissions of AeroGas Turbine Combustion with Synthetic Kerosens. Honors Undergraduate Thesis. Statesboro: Georgia Southern University.

Kärcher, B. "The Importance of Contrail Ice Formation for Mitigating the Climate Impact of Aviation." *Journal of Geophysical Research: Atmospheres* 121, no. 7 (2016): 3497–3505. https://doi.org/10.1002/2015jd024696.

Lee, David S., David W. Fahey, Piers M. Forster, Peter J. Newton, Ron C.N. Wit, Ling L. Lim, Bethan Owen, and Robert Sausen. "Aviation and Global Climate Change in the 21st Century." *Atmospheric Environment* 43, no. 22-23 (2009): 3520–37. https://doi.org/10.1016/j.atmosenv.2009.04.024.

Liu, Guangrui, Beibei Yan, and Guanyi Chen. "Technical Review on Jet Fuel Production." *Renewable and Sustainable Energy Reviews* 25 (2013): 59–70. https://doi.org/10.1016/j.rser.2013.03.025.

Mahashabde, Anuja, Philip Wolfe, Akshay Ashok, Christopher Dorbian, Qinxian He, Alice Fan, Stephen Lukachko, et al. "Assessing the Environmental Impacts of Aircraft Noise and Emissions." *Progress in Aerospace Sciences* 47, no. 1 (2011): 15–52. https://doi.org/10.1016/j.paerosci.2010.04.003.

Mathews, D. C., and N. F. Rekos. "Prediction and Measurement of Direct Combustion Noise in Turbopropulsion Systems." *Journal of Aircraft* 14, no. 9 (1977): 850–59. https://doi.org/10.2514/3.58865.

Measuring Sound. (1984). Accessed 3 29, 2022, from Bruel and Kjaer Sound & Vibration Measurement A/S: https://www.bksv.com/media/doc/br0047.pdf

"MKS FTIR MultiGas™ 2030 Emissions Analyzer." Environmental Analysis Solutions. MKS Instruments Inc., 2017. https://www.mksinst.com/mam/celum/celum_assets/resources/onlinemultigas2030ds.pdf.

NASA. Contrails. Aeronautics Research Mission Directorate. Accessed 2022. https://www.nasa.gov/sites/default/files/atoms/files/contrails_k-12.pdf#:~:text=Contrails%20are%20a%20type%20of%20ice%20cloud%2C%20formed,of%20soot%20particles%20produced%20during%20the%20combustion%20process.?msclkid=6c36be6aa98111ecaa9a7aa403f142c5

"Octave Analysis: Dewesoft X Manual." Octave Analysis > Frequency Domain Analysis > Math > General > Modules > Setup | Dewesoft X Manual EN. DEWESoft. Accessed March 24, 2022. https://manual.dewesoft.com/x/setupmodule/modules/general/math/freqdomainanalysis/cpb.

Overton, Jeff. "Fact Sheet: The Growth in Greenhouse Gas Emissions from Commercial Aviation (2019)." EESI. Environmental and Energy Study Institute (EESI), 2019. https://www.eesi.org/papers/view/fact-sheet-the-growth-in-greenhouse-gas-emissions-from-commercial-aviation.

Phillips, C. (2020). An Investigative Study of Combustion and Emissions with Noise and Vibrations Of Synthetic Fuels within an Aero-Gas Turbine. Honors Undergraduate Thesis. Statesboro: Georgia Southern University. https://digitalcommons.georgiasouthern.edu/honors-theses/538/

Potter, Wendell, and David Webb. "2. Wave Properties and Characteristics." Physics LibreTexts. Libretexts, July 27, 2020. https://phys.libretexts.org/Courses/University_of_California_Davis/UCD%3A_Physics_7C_-_General_Physics/08._Waves/8.1%3A_Introduction_to_Waves/2._Wave_Properties_and_Characteristics.

Ra, Ho Won, Tae-Young Mun, Sung Jun Hong, Dong Hyun Chun, Ho Tae Lee, Sung Min Yoon, Ji Hong Moon, et al. "Indirect Coal Liquefaction by Integrated Entrained Flow Gasification and Rectisol/Fischer–Tropsch Processes for Producing Automobile Diesel Substitutes." *Energy* 219 (2021): 119597. https://doi.org/10.1016/j.energy.2020.119597.

Randall, Randolph B. *Frequency Analysis*. Naerum: Brüel et Kjaer, 1987.

Riebl, Sebastian, Marina Braun-Unkhoff, and Uwe Riedel. "A Study on the Emissions of Alternative Aviation Fuels." *Journal of Engineering for Gas Turbines and Power* 139, no. 8 (2017). https://doi.org/10.1115/1.4035816.

Satcher, David. *Toxicological Profile for Jet Fuels JP-4 and JP-7: Draft*. Washington, D.C.: U.S. Dept. of Health and Human Services, 1993.

Schaufele, Roger, and Michael Lukacs. "FAA Aerospace Forecast." FAA Aerospace Forecast Fiscal Years 2021-2041. Forecasts and Performance Analysis Division (APO-100), Office of Aviation Policy and Plans, 2021. https://www.faa.gov/data_research/aviation/aerospace_forecasts/media/FY2021-41_FAA_Aerospace_Forecast.pdf.

Schwarz, Anna, and Johannes Janicka. *Combustion Noise*. Berlin: Springer Berlin, 2014.

Selam, Muaz, Wajdi Ahmed, Moiz Bohra, Hafis Mohamed, Rehan Hussain, and Nimir Elbashir. "Role of Aromatics in Synthetic Fuels." *Qatar Foundation Annual Research Conference Proceedings Volume 2014 Issue 1*, 2014. https://doi.org/10.5339/qfarc.2014.eesp0487.

Simons, E. (2016). Electronic Theses and Dissertations. Retrieved 6 20, 2020, from Investigations of the Combustion Sound and Vibration Characteristics of an Aeroderivative Gas Turbine: https://digitalcommons.georgiasouthern.edu/etd/151

Tao, W., M. Mazur, M. Huet, and F. Richecoeur. "Indirect Combustion Noise Contributions in a Gas Turbine Model Combustor with a Choked Nozzle." *Combustion Science and Technology* 188, no. 4-5 (2016): 793–804. https://doi.org/10.1080/00102202.2016.1139374.

Turbine Technologies, LTD. 2011. *Minilab Gas Turbine Power System Operator's Manual.* Chetek, 2011. Accessed 3 27, 2022.

"What Is the Greenhouse Effect?" American Chemical Society, 2022. https://www.acs.org/content/acs/en/climatescience/climatesciencenarratives/what-is-the-greenhouse-effect.html.